
Volume 58 Issue 10 October 2010 ISSN 0022-5096

ELSEVIER

JOURNAL OF THE
MECHANICS AND PHYSICS
OF SOLIDS

Journal of the Mechanics and Physics of Solids 58 (2010) 1524–1551

Contents lists available at ScienceDirect

Journal of the Mechanics and Physics of Solids

journal homepage: www.elsevier.com/locate/jmps

Theory of indentation on multiferroic composite materials

Weiqiu Chen [a], Ernian Pan [b,*], Huiming Wang [a], Chuanzeng Zhang [c]

[a] Department of Engineering Mechanics, Zhejiang University, Yuquan Campus, Hangzhou 310027, PR China
[b] Department of Civil Engineering and Department of Applied Mathematics, University of Akron, Akron, OH 44326-3905, USA
[c] Department of Civil Engineering, University of Siegen, D-57068 Siegen, Germany

ARTICLE INFO

Article history:
Received 22 March 2010
Received in revised form
7 June 2010
Accepted 14 July 2010

Keywords:
Indentation
Half-space Green's functions
Transverse isotropy
Magneto-electro-elastic
Multiferroic composite

ABSTRACT

This article presents a general theory on indentation over a multiferroic composite half-space. The material is transversely isotropic and magneto-electro-elastic with its axis of symmetry normal to the surface of the half-space. Based on the corresponding half-space Green's functions to point sources applied on the surface, explicit expressions for the generalized pressure vs. indentation depth are derived *for the first time* for the three common indenters (flat-ended, conical, and spherical punches). The important multiphase coupling issue is discussed in detail, with the weak and strong coupling being correctly revisited. The derived analytical solutions of indentation will not only serve as benchmarks for future numerical studies of multiphase composites, but also have important applications to experimental test and characterization of multiphase materials, in particular, of multiferroic properties.

1. Introduction

Study on magneto-electro-elastic (MEE) and/or multiferroic materials/composites has recently emerged as an important topic in various research communities because of the great potential applications of these materials and related devices to edge-cutting technologies (Spaldin and Fiebig, 2005; Nan et al., 2008). The multi-couplings among elastic, electric and magnetic fields in multiferroic materials also present a challenge on the theoretical analysis associated with the magnetoelectric (ME) effect (Nan, 1994; Benveniste, 1995; Wu and Huang, 2000), effective properties of composites (Li and Dunn, 1998), static and dynamic structural behaviors (Pan, 2001; Chen and Lee, 2003), fractures (Liu et al., 2001; Sih and Chen, 2003; Feng et al., 2007), Green's functions and other mathematical aspects of the coupled theory (Pan, 2002; Wang and Shen, 2002; Li, 2003; Hou et al., 2005; X. Wang et al., 2008).

Indentation technique has been widely employed to characterize mechanical and/or electric properties of advanced and layered materials (Lawn and Wilshaw, 1975; Gao et al., 1992; Kalinin and Bonnell, 2002; Vlassak et al., 2003; Kalinin et al., 2007b). This technique obviously relies on the solutions of the corresponding contact mechanics (Sneddon, 1965). For earlier developments, readers are referred to Gladwell (1980), Johnson (1985) and Sackfield et al. (1993), to name a few. A simple and conceptually straightforward method was also proposed by Yu (2001) for the study of various boundary-value problems (e.g. the frictionless normal indentation, prescribed surface tractions, sliding contact, and the adhesive punch) in a transversely isotropic half-space.

With the broad use of piezoelectric ceramics in various engineering applications, it is important to characterize their material properties. Giannakopoulos and Suresh (1999) presented a general theory of indentation of piezoelectric materials: they derived the relations between the generalized pressure and indentation depth by using the Hankel

* Corresponding author. Tel.: +1 330 972 6739; fax: +1 330 972 6020.
E-mail address: pan2@uakron.edu (E. Pan).

0022-5096/$ - see front matter © 2010 Elsevier Ltd. All rights reserved.
doi:10.1016/j.jmps.2010.07.012

transform for the three typical indenters as shown in Fig. 1. Giannakopoulos (2000) also used the indentation technique for determining the strength of piezoelectric materials. Concurrently, Chen and Ding (1999), Chen et al. (1999) and Chen (2000) conducted a series of investigations on the contact problems of spherical, conical and flat-ended punches on a transversely isotropic piezoelectric half-space by using Fabrikant's method in potential theory (Fabrikant, 1989, 1991), which was further successfully used for the elastic solutions of several very important indentation problems by Hanson (1992a,b). They obtained the complete and exact three-dimensional (3D) expressions for the electroelastic field in the half-space in terms of elementary functions, and further found that, for conical and spherical indenters, although the mechanical penetration does not induce a singular stress at the edge of contact, an additional application of a non-zero constant potential to the indenter would lead to a usual square-root singularity in the induced stress field at the edge of contact (Chen and Ding, 1999; Chen et al., 1999; Chen, 2000). This was later confirmed by Kalinin et al. (2004) and Karapetian et al. (2005), who employed the correspondence principle developed in Karapetian et al. (2002). However, such a stress singularity phenomenon was not observed in Giannakopoulos and Suresh (1999) and Yang (2008), both employed the Hankel transform. The difference between the results obtained by different methods is still unclear up to now.

Recently, J.H. Wang et al. (2008) presented an interesting study on the indentation of piezoelectric thin films by using the Hankel transform. They derived some useful empirical formulae based on comprehensive numerical simulations. Exciting works led by Kalinin (Kalinin et al., 2004; Karapetian et al., 2005; Kalinin et al., 2007b) have further shown the importance of exact 3D contact solutions in interpreting quantitatively the responses of various scanning probe microscopies (SPM). They recently considered the indentation of piezoelectric materials by flat and non-flat punches of arbitrary planform (Karapetian et al., 2009).

Giannakopoulos and Parmaklis (2007) conducted a parallel study on piezomagnetic materials by employing the Hankel transform. They showed that the coupling between the elastic and magnetic fields would lead to a significant effect on the indentation force. They also conducted an experimental study by using Terfenol-D material and compared both their testing results and theoretical predictions.

There are only a few works on contact mechanics of MEE or multiferroic materials. Hou et al. (2003) presented exact solutions of elliptical Hertzian contact of MEE bodies for both smooth and frictional contact cases. Their work is an extension

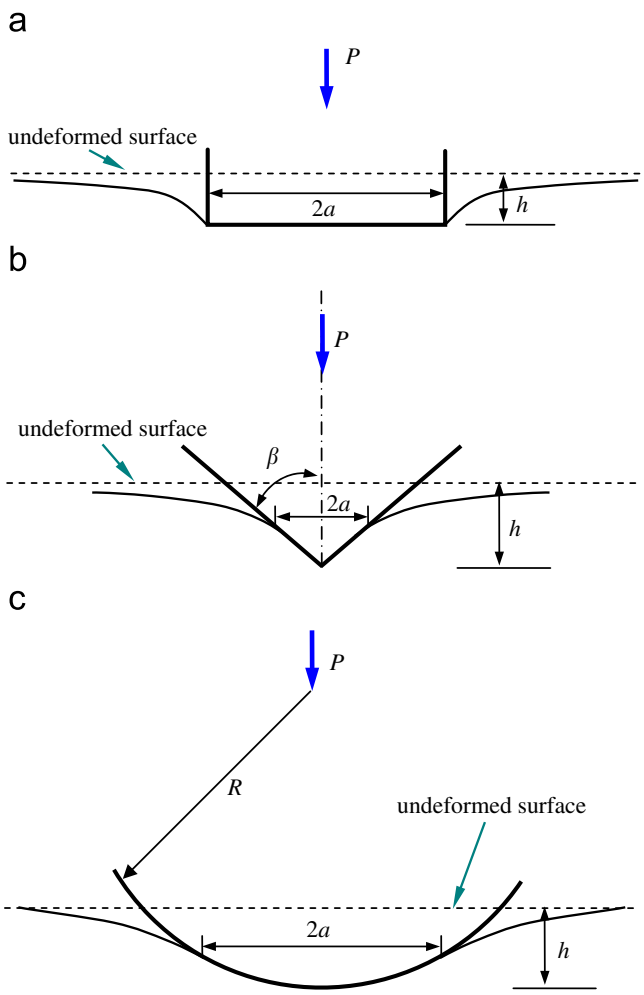

Fig. 1. Three common indenters: (a) a flat-ended circular punch, (b) a circular cone, and (c) a sphere. P denotes the total mechanical force, a the contact radius, and h the indentation depth.

of Hanson and Puja (1997) for the corresponding transversely isotropic elastic materials based on the method in potential theory developed by Fabrikant (1989). However, the results obtained in Hou et al. (2003), although mathematically beautiful, are somehow complicated because of the elliptical geometry considered. As such, some important issues related to the magnetoelectric properties of the indenter could not be addressed. For most applications, indenters are axisymmetric and usually have a much simpler shape than the elliptical one. Shown in Fig. 1 are the three common indenters, i.e. the flat-ended cylindrical punch, the conical punch and the spherical punch. With the rapid developments of multiferroic materials, structures and devices, it is hence very important to develop a theory on the contact mechanics between the indenters and multiferroic materials, not to mention that the corresponding work on piezoelectric materials has already stimulated very broad interests in research and applications (see, for example, Kalinin et al., 2007b).

Motivated by the potential broad and important applications of multiferroic materials and composites, we present in this paper, the basic theory of indentation on these materials/composites. We first present the governing equations and the corresponding half-space Green's function of surface sources in transversely isotropic MEE materials in Section 2. In Section 3, we present the exact solutions for the three common indenters (flat-ended, conical, and spherical punches, see Fig. 1). The important multiphase coupling issue is analyzed through numerical examples and the reduced uncoupled results are discussed in Section 4, contributing further on clarifying the controversial stress singularity issue at the contact edge. Finally in Section 5, we summarize our results and discuss also their potential future applications.

2. Governing equations and half-space Green's function in transversely isotropic MEE materials

We introduce the cylindrical coordinates (r, θ, z) with the $r-\theta$ plane parallel to the plane of isotropy of the transversely isotropic MEE material. The origin of the z-coordinate is on the surface and the z-axis points into the half-space. In this system, the generalized constitutive relations are (Chen et al., 2004)

$$\begin{aligned}
\sigma_{rr} &= c_{11}s_{rr}+c_{12}s_{\theta\theta}+c_{13}s_{zz}-e_{31}E_z-q_{31}H_z,\\
\sigma_{\theta\theta} &= c_{12}s_{rr}+c_{11}s_{\theta\theta}+c_{13}s_{zz}-e_{31}E_z-q_{31}H_z,\\
\sigma_{zz} &= c_{13}s_{rr}+c_{13}s_{\theta\theta}+c_{33}s_{zz}-e_{33}E_z-q_{33}H_z,\\
\sigma_{\theta z} &= 2c_{44}s_{\theta z}-e_{15}E_\theta-q_{15}H_\theta,\\
\sigma_{rz} &= 2c_{44}s_{rz}-e_{15}E_r-q_{15}H_r,\\
\sigma_{r\theta} &= 2c_{66}s_{r\theta},
\end{aligned} \tag{1a}$$

$$\begin{aligned}
D_r &= 2e_{15}s_{rz}+\varepsilon_{11}E_r+d_{11}H_r,\\
D_\theta &= 2e_{15}s_{\theta z}+\varepsilon_{11}E_\theta+d_{11}H_\theta,\\
D_z &= e_{31}(s_{rr}+s_{\theta\theta})+e_{33}s_{zz}+\varepsilon_{33}E_z+d_{33}H_z,
\end{aligned} \tag{1b}$$

$$\begin{aligned}
B_r &= 2q_{15}s_{rz}+d_{11}E_r+\mu_{11}H_r,\\
B_\theta &= 2q_{15}s_{\theta z}+d_{11}E_\theta+\mu_{11}H_\theta,\\
B_z &= q_{31}(s_{rr}+s_{\theta\theta})+q_{33}s_{zz}+d_{33}E_z+\mu_{33}H_z,
\end{aligned} \tag{1c}$$

where σ_{ij}, D_i, and B_i are the stresses, electric displacements, and magnetic inductions (i.e., magnetic fluxes), respectively; s_{ij}, E_i, and H_i are the strains, electric fields and magnetic fields, respectively; c_{ij}, ε_{ij}, and μ_{ij} are the elastic, dielectric, and magnetic permeability coefficients, respectively; e_{ij}, q_{ij}, and d_{ij} are the piezoelectric, piezomagnetic, and magnetoelectric coefficients, respectively. For the transversely isotropic material, we also have $c_{66}=(c_{11}-c_{12})/2$. It is obvious that various decoupled cases can be reduced from Eq. (1) by setting the appropriate coupling coefficients to zero. This, as well as the weakly and strongly coupled cases, will be addressed later.

The strain–elastic displacement, electric field-potential, and magnetic field-potential relations are

$$\begin{aligned}
&s_{rr}=\frac{\partial u_r}{\partial r},\quad s_{\theta\theta}=\frac{1}{r}\frac{\partial u_\theta}{\partial\theta}+\frac{u_r}{r},\quad s_{zz}=\frac{\partial u_z}{\partial z},\quad s_{\theta z}=\frac{1}{2}\left(\frac{\partial u_\theta}{\partial z}+\frac{1}{r}\frac{\partial u_z}{\partial\theta}\right),\\
&s_{rz}=\frac{1}{2}\left(\frac{\partial u_z}{\partial r}+\frac{\partial u_r}{\partial z}\right),\quad s_{r\theta}=\frac{1}{2}\left(\frac{1}{r}\frac{\partial u_r}{\partial\theta}+\frac{\partial u_\theta}{\partial r}-\frac{u_\theta}{r}\right),
\end{aligned} \tag{2a}$$

$$E_r=-\frac{\partial\phi}{\partial r},\quad E_\theta=-\frac{1}{r}\frac{\partial\phi}{\partial\theta},\quad E_z=-\frac{\partial\phi}{\partial z}, \tag{2b}$$

$$H_r=-\frac{\partial\psi}{\partial r},\quad H_\theta=-\frac{1}{r}\frac{\partial\psi}{\partial\theta},\quad H_z=-\frac{\partial\psi}{\partial z}, \tag{2c}$$

where u_i, ϕ, and ψ are the elastic displacement, electric potential, and magnetic potential, respectively.

In the cylindrical coordinate system, the generalized equilibrium equations for the system free of any body sources are

$$\begin{aligned}
&\frac{\partial\sigma_{rr}}{\partial r}+\frac{1}{r}\frac{\partial\sigma_{r\theta}}{\partial\theta}+\frac{\partial\sigma_{rz}}{\partial z}+\frac{\sigma_{rr}-\sigma_{\theta\theta}}{r}=0,\\
&\frac{\partial\sigma_{r\theta}}{\partial r}+\frac{1}{r}\frac{\partial\sigma_{\theta\theta}}{\partial\theta}+\frac{\partial\sigma_{\theta z}}{\partial z}+\frac{2\sigma_{r\theta}}{r}=0,
\end{aligned}$$

$$\frac{\partial\sigma_{rz}}{\partial r}+\frac{1}{r}\frac{\partial\sigma_{\theta z}}{\partial\theta}+\frac{\partial\sigma_{zz}}{\partial z}+\frac{\sigma_{rz}}{r}=0, \tag{3a}$$

$$\frac{\partial D_r}{\partial r}+\frac{1}{r}\frac{\partial D_\theta}{\partial\theta}+\frac{\partial D_z}{\partial z}+\frac{D_r}{r}=0, \tag{3b}$$

$$\frac{\partial B_r}{\partial r}+\frac{1}{r}\frac{\partial B_\theta}{\partial\theta}+\frac{\partial B_z}{\partial z}+\frac{B_r}{r}=0. \tag{3c}$$

If we assume that there is a vertical force P, point electric charge Q, and magnetic "charge" M (electric current) applied at the origin on the surface, then the problem is axisymmetric with $u_\theta=0$ and $\partial/\partial\theta=0$. Denoting $P_1=P$, $P_2=-Q$ and $P_3=-M$, we then find the point-source Green's functions as (Hou et al., 2003, 2005)

$$\begin{aligned}&u_r(r,z)=-\sum_{i=1}^{4}A_i\frac{r}{R_iR_i^*},\quad w_k(r,z)=\sum_{i=1}^{4}\alpha_{ik}A_i\frac{1}{R_i},\quad \sigma_{zl}(r,z)=-\sum_{i=1}^{4}\gamma_{il}A_i\frac{z_i}{R_i^3},\\&\tau_{zk}(r,z)=-\sum_{i=1}^{4}\gamma_{ik}s_iA_i\frac{r}{R_i^3},\quad \sigma_2(r,z)=2c_{66}\sum_{i=1}^{4}A_i\frac{r^2}{R_i^2R_i^*}\left(\frac{1}{R_i}+\frac{1}{R_i^*}\right),\end{aligned} \tag{4}$$

where $k=1, 2, 3$ and $l=1, 2, 3, 4$, $R_i=\sqrt{r^2+z_i^2}$, $R_i^*=R_i+z_i$, $z_j=s_jz$, and s_i ($i=1, 2, 3, 4$) are the four roots (eigenvalues) with positive real parts, which are assumed distinct in this paper, of the characteristic equation given in Appendix A. For the case of equal eigenvalues, its analysis is similar to Chen (2000) for piezoelectric materials. Furthermore, in writing the compact solution (4), we have introduced the following notations:

$$\begin{aligned}&w_1=u_z,\quad w_2=\phi\quad w_3=\psi,\\&\sigma_{z1}=\sigma_{zz},\quad \sigma_{z2}=D_z,\quad \sigma_{z3}=B_z,\quad \sigma_{z4}=\sigma_{rr}+\sigma_{\theta\theta},\quad \sigma_2=\sigma_{rr}-\sigma_{\theta\theta},\\&\tau_{z1}=\sigma_{rz},\quad \tau_{z2}=D_r,\quad \tau_{z3}=B_r,\end{aligned} \tag{5}$$

and the material constants in Eq. (4) are given by

$$\begin{aligned}&\gamma_{i1}=c_{13}+c_{33}s_i\alpha_{i1}+e_{33}s_i\alpha_{i2}+q_{33}s_i\alpha_{i3},\\&\gamma_{i2}=e_{31}+e_{33}s_i\alpha_{i1}-\varepsilon_{33}s_i\alpha_{i2}-d_{33}s_i\alpha_{i3},\\&\gamma_{i3}=q_{31}+q_{33}s_i\alpha_{i1}-d_{33}s_i\alpha_{i2}-\mu_{33}s_i\alpha_{i3},\\&\gamma_{i4}=2[(c_{11}-c_{66})+c_{13}s_i\alpha_{i1}+e_{31}s_i\alpha_{i2}+q_{31}s_i\alpha_{i3}],\end{aligned} \tag{6}$$

where α_{ij} are defined in Appendix A, and the coefficients A_i in Eq. (4) are determined from the boundary conditions at $z=0$ as well as the generalized force equilibrium condition (Hou et al., 2003); they can be expressed as $A_i=\sum_{j=1}^{3}I_{ij}P_j$, where

$$\begin{Bmatrix}I_{1j}\\I_{2j}\\I_{3j}\\I_{4j}\end{Bmatrix}=\frac{1}{2\pi}\begin{bmatrix}\gamma_{11}s_1&\gamma_{21}s_2&\gamma_{31}s_3&\gamma_{41}s_4\\\gamma_{11}&\gamma_{21}&\gamma_{31}&\gamma_{41}\\\gamma_{12}&\gamma_{22}&\gamma_{32}&\gamma_{42}\\\gamma_{13}&\gamma_{23}&\gamma_{33}&\gamma_{43}\end{bmatrix}^{-1}\begin{Bmatrix}0\\\delta_{1j}\\\delta_{2j}\\\delta_{3j}\end{Bmatrix}, \tag{7}$$

where δ_{ij} is the Kronecker delta. It can be seen from Eq. (4) that the Green's functions for point sources applied on the boundary of a half-space are expressed exactly and explicitly in terms of elementary functions. This will be greatly beneficial to the succeeding analysis of contact problems.

Denoting $\xi_{kj}=\sum_{i=1}^{4}\alpha_{ik}I_{ij}$, we have the following important relation:

$$\xi_{kj}=\xi_{jk}, \tag{8}$$

which can be verified by direct substitution. This result follows from the reciprocity theorem as presented in Appendix B.

3. Boundary value problems and fundamental results of indentation on a MEE half-space

3.1. Boundary conditions and integral expression

It is obvious that, for a given indentation problem, the field quantities should vanish at infinity. This has been automatically satisfied by the Green's functions given in Eq. (4). Thus, only the conditions on the boundary surface $z=0$ should be considered. As for the boundary value problems for the three common indenters shown in Fig. 1(a)–(c), we discuss them separately in terms of their mechanical, electric, and magnetic conditions.

For the mechanical boundary conditions, we have

$$0\le r\le a:\begin{cases}u_z(r,0)=h, & \text{for flat},\\u_z(r,0)=h-r\cot\beta, & \text{for cone},\\u_z(r,0)=h-r^2/(2R), & \text{for sphere},\end{cases} \tag{9a}$$

$$r \geq 0 : \sigma_{rz}(r,0) = 0, \tag{9b}$$

$$r > a : \sigma_{zz}(r,0) = 0, \tag{9c}$$

where h is the indentation depth, a the radius of the circular contact area, β the half apex angle of the conical indenter, and R the radius of the spherical indenter.

For the electric boundary conditions, we have for the three indenters:

(a) For a perfect electric conducting indenter with constant electric potential ϕ_0:

$$0 \leq r < a : \ \phi(r,0) = \phi_0, \qquad r > a : \ D_z(r,0) = 0. \tag{10}$$

(b) For an indenter as a perfect electric insulator with zero electric charge:

$$r \geq 0 : D_z(r,0) = 0. \tag{11}$$

For the magnetic boundary conditions, we have, for the three indenters, similarly:

(a) For a perfect magnetic conducting indenter with constant magnetic potential ψ_0:

$$0 \leq r < a : \ \psi(r,0) = \psi_0, \qquad r > a : \ B_z(r,0) = 0. \tag{12}$$

(b) For an indenter as a perfect magnetic insulator with zero magnetic flux:

$$r \geq 0 : \ B_z(r,0) = 0. \tag{13}$$

By the method of superposition, the indentation (generalized) displacements (vertical elastic displacement, and electric and magnetic potentials) can be expressed in terms of integrals over the indenter area S $(0 \leq r \leq a)$ of the unknown pressure distribution and the unknown or known electric charge or magnetic flux, which depends on the indenter's electromagnetic properties, as discussed above. This leads to

$$w_k(r,\theta,0) = \sum_{j=1}^{3} \xi_{kj} \int_0^{2\pi} \int_0^a \frac{p_j(\rho,\theta_0)}{R_0} \rho \, d\rho \, d\theta_0 \quad (k = 1,2,3), \tag{14}$$

where R_0 is the distance between the two surface points $(r, \theta, 0)$ and $(\rho, \theta_0, 0)$ defined as $R_0 = \sqrt{r^2 + \rho^2 - 2r\rho\cos(\theta - \theta_0)}$, and

$$p_k(r,\theta) = -\sigma_{zk}(r,\theta,0) \quad (k = 1,2,3). \tag{15}$$

For axisymmetric problems, both w_k and p_k (k=1, 2, 3) are independent of the angle θ. However, we still keep this variable in Eq. (14) so that the governing equations have the same structure as that in Fabrikant (1989, 1991), whose results then will be employed here. Also, occasionally we may write $p_k(r, \theta)$=$p_k(r)$ or simply p_k for brevity.

3.2. Solution for electrically and magnetically conducting indenters

First, we assume that all the three "pressures" p_k (k=1, 2, 3) are unknowns, i.e. the indenter is electrically and magnetically conducting. From Eq. (14), we obtain

$$\int_0^{2\pi} \int_0^a \frac{p_j(\rho,\theta_0)}{R_0} \rho \, d\rho \, d\theta_0 = \frac{1}{\eta} \sum_{k=1}^{3} \eta_{kj} w_k(r,\theta,0) \quad (j = 1,2,3) \tag{16}$$

where $\eta = |\xi_{kj}|$ is the determinant, and η_{kj} are the corresponding cofactors. In view of Eq. (8), we have

$$\eta_{kj} = \eta_{jk}. \tag{17}$$

The integral equations, Eq. (16), then can be solved using either the well-known property of Abel operator or the existing results in the potential theory. Here we use the results of Fabrikant (1989) and Hanson (1992a,b). While we omit the detailed derivation, some key steps are listed in Appendix C for easy reference. We remark that although a very similar derivation for piezoelectric materials can be found in Chen and Ding (1999), Chen et al. (1999), and Chen (2000), here in this paper a different condition (i.e., total stress field vanishes at the contact edge) for the determination of the contact radius of the conical or spherical indenter is used, leading to a quite different result than that in Chen and Ding (1999) and Chen et al. (1999) even for a piezoelectric material. This alternative condition was also employed by Giannakopoulos and Suresh (1999), Yang (2008), and J.H. Wang et al. (2008) for piezoelectric materials. After solving the integral equations (16), we can obtain the following important results for the three common indenters.

3.2.1. Flat indenter

The pressure, normal electric displacement, and normal magnetic flux distributions under the flat indenter are

$$p_j(r,\theta) = \frac{\eta_{1j} h + \eta_{2j}\phi_0 + \eta_{3j}\psi_0}{\pi^2 \eta} \frac{1}{\sqrt{a^2 - r^2}} \quad (j = 1,2,3). \tag{18}$$

Note that $\sigma_{zz}(r, \theta, 0) = -p_1(r)$, $D_z(r, \theta, 0) = -p_2(r)$ and $B_z(r, \theta, 0) = -p_3(r)$. As expected, for a flat indenter, the constant displacement, electric potential, and magnetic potential play a similar role. Just like the purely elastic case (Fabrikant, 1989), the normal stress is infinite at the edge of the contact area (i.e. $r=a$), exhibiting a square-root singularity. The electric displacement and magnetic flux also have the same singularity at $r=a$.

The resultant indentation force, total electric charge, and total magnetic flux are

$$P_j = 2\pi \int_0^a p_j(r) r\, dr = \frac{2a(\eta_{1j}h + \eta_{2j}\phi_0 + \eta_{3j}\psi_0)}{\pi\eta} \quad (j = 1,2,3). \tag{19}$$

Note that the resultant indentation force $P=P_1$, the total electric charge $Q=-P_2$ and the total magnetic charge $M=-P_3$ as introduced in Section 2, Eq. (19) may be rewritten as

$$\begin{Bmatrix} P \\ Q \\ M \end{Bmatrix} = \frac{2a}{\pi} \begin{bmatrix} \frac{\eta_{11}}{\eta} & \frac{\eta_{21}}{\eta} & \frac{\eta_{31}}{\eta} \\ -\frac{\eta_{12}}{\eta} & -\frac{\eta_{22}}{\eta} & -\frac{\eta_{32}}{\eta} \\ -\frac{\eta_{13}}{\eta} & -\frac{\eta_{23}}{\eta} & -\frac{\eta_{33}}{\eta} \end{bmatrix} \begin{Bmatrix} h \\ \phi_0 \\ \psi_0 \end{Bmatrix} \equiv \frac{2a}{\pi}\mathbf{C} \begin{Bmatrix} h \\ \phi_0 \\ \psi_0 \end{Bmatrix} \equiv \mathbf{G} \begin{Bmatrix} h \\ \phi_0 \\ \psi_0 \end{Bmatrix}. \tag{20}$$

Normally one can define the indentation stiffness as a variation ratio $\delta P/\delta h$ at constant electric and magnetic potentials, and hence the element G_{11} represents just the indentation stiffness coefficient. Similarly, G_{12} corresponds to the indentation piezoelectric coefficient, G_{13} the indentation piezomagnetic coefficient, G_{22} the indentation dielectric coefficient, G_{23} the indentation magnetoelectric coefficient, and G_{33} the indentation magnetic permeability coefficient. Thus, Eq. (20) provides various stiffness relations (or the global constitutive relations) of the indenter, and the matrix $\mathbf{G} = [G_{ij}] = (2a/\pi)[C_{ij}]$ may be termed as the generalized indentation stiffness matrix. Note that such a definition of generalized stiffness coefficients exactly follows Yang (2008), but is clearly different from that in Kalinin et al. (2004) and Karapetian et al. (2005) by the factor of $2a/\pi$, which represents the geometric effect of the indenter. In fact, in the piezoelectric case, the corresponding elements in $\mathbf{C}$ were used by Kalinin et al. (2004) and Karapetian et al. (2005) as various indentation constants. For the flat-ended indenter, either $\mathbf{G}$ or $\mathbf{C}$ can be seen as the indentation stiffness matrix since the contact radius a is prescribed and does not change during indentation. From Eq. (17), we obtain the following three interesting relations:

$$C_{12} = -C_{21}, \quad C_{13} = -C_{31}, \quad C_{23} = C_{32}, \tag{21}$$

with the first one being observed by Kalinin et al. (2004) for a piezoelectric half-space, and proved later through a rather complicated derivation (Kalinin et al., 2007a). As mentioned earlier and detailed in Appendix B, these relations stem from the reciprocity pertinent to the linear theory of magneto-electro-elasticity. It is further interesting to note that, the factor $2a/\pi$ also appears in the stiffness relations for any axisymmetric indenter. While this factor is fixed for a flat indenter, it varies with the total force exerted on the conical or spherical indenter to be considered below and depends further on the material properties of the half-space.

The indentation depth is found as

$$h = \frac{1}{\eta_{11}}\left[\frac{\pi\eta P}{2a} - (\eta_{21}\phi_0 + \eta_{31}\psi_0)\right], \tag{22}$$

which is expressed in terms of the resultant force, and the prescribed electric and magnetic potentials. It is obtained directly from the first equation in Eq. (19). From this relation, it is clear that the indentation depth can be conveniently adjusted by imposing a proper electric or magnetic potential on the conducting indenter, a feature could be very useful in indentation test of multiferroic materials.

The complete and exact 3D expressions for the MEE field in the half-space are presented in Appendix D. These are particularly useful in evaluating the material failure strength by the indentation technology, estimating the resolution of electromagnetic microscopy, or interpreting the polarization switching behavior in multiferroic materials (Kalinin et al., 2004), which is especially important in developing new devices of high-density and high-performance memories.

3.2.2. Conical indenter

The pressure, normal electric displacement, and normal magnetic flux distributions under the conical indenter are:

$$p_j(r) = \frac{\eta_{1j}\cot\beta}{2\pi\eta}\cosh^{-1}\left(\frac{a}{r}\right) + \frac{\eta_{1j}(h - \pi a\cot\beta/2) + \eta_{2j}\phi_0 + \eta_{3j}\psi_0}{\pi^2\eta}\frac{1}{\sqrt{a^2 - r^2}} \quad (j = 1,2,3), \tag{23}$$

Compared to the flat indenter (18), the conical indenter causes very different distributions of the pressure, normal electric displacement and magnetic flux under the indenter since the conical shape induces a non-uniform mechanical indentation. It is interesting to note, however, that the normal stress is no longer singular at $r=a$, as required in obtaining the solution, see Appendix C. In fact, by utilizing the relation in Eq. (26) below, we obtain from Eq. (23) that

$$p_1(r) = \frac{\eta_{11}\cot\beta}{2\pi\eta}\cosh^{-1}\left(\frac{a}{r}\right),$$

which gives $p_1(a)=0$. On the other hand, a logarithmic singularity in the stress field appears at $r=0$ due to the sharpness of the conical apex (Hanson, 1992a; Chen et al., 1999). As for the electric and magnetic fields, they still exhibit the common square-root singularity at $r=a$ due to the discontinuity in the surface electric/magnetic potentials across the edge of the contact.

The resultant indentation force, total electric charge, and total magnetic flux are:

$$P_j=\frac{a}{\pi\eta}\left[\eta_{1j}h+\left(2\eta_{2j}-\frac{\eta_{1j}\eta_{21}}{\eta_{11}}\right)\phi_0+\left(2\eta_{3j}-\frac{\eta_{1j}\eta_{31}}{\eta_{11}}\right)\psi_0\right]\quad (j=1,2,3), \tag{24}$$

which can also be rewritten in the form of Eq. (20), but with a different **C** matrix

$$\mathbf{C}=\frac{1}{\eta}\begin{bmatrix}\frac{1}{2}\eta_{11} & \frac{1}{2}\eta_{21} & \frac{1}{2}\eta_{31}\\ -\frac{1}{2}\eta_{12} & \frac{1}{2}\frac{\eta_{12}^2}{\eta_{11}}-\eta_{22} & \frac{1}{2}\frac{\eta_{12}\eta_{31}}{\eta_{11}}-\eta_{32}\\ -\frac{1}{2}\eta_{13} & \frac{1}{2}\frac{\eta_{21}\eta_{13}}{\eta_{11}}-\eta_{23} & \frac{1}{2}\frac{\eta_{31}^2}{\eta_{11}}-\eta_{33}\end{bmatrix}. \tag{25}$$

The symmetry relations (21) still hold. In deriving Eq. (24), we have utilized the relation in Eq. (26) below. In spite of the additional magnetic field, relation (24) looks just like that derived by Karapetian et al. (2005) for a piezoelectric half-space. However, even with proper degeneration procedures as outlined in Appendix E, our relation will not be identical to that in Karapetian et al. (2005) for the piezoelectric half-space since a different condition on vanishing stress singularity at the contact edge is used here. It is also noted that, for the conical indenter, the contact radius a depends not only on the total pressure, but also on the material properties of the half-space (see Eq. (27) below). From Eqs. (24) and (26), we can calculate

$$\left.\frac{\delta P}{\delta h}\right|_{\phi_0,\psi_0}=\frac{2a\eta_{11}}{\pi\eta},\quad \left.\frac{\delta P}{\delta \phi_0}\right|_{h,\psi_0}=\frac{2a\eta_{21}}{\pi\eta},\quad \left.\frac{\delta P}{\delta \psi_0}\right|_{h,\phi_0}=\frac{2a\eta_{31}}{\pi\eta},$$

which show that the elements G_{11}, G_{12} and G_{13} in matrix **G** coincide with the indentation coefficients defined above except for a factor 2. However, further calculation shows that the other elements in **G** no longer bear the same physical essences as those defined before. For example, we have

$$\left.\frac{\delta Q}{\delta h}\right|_{\phi_0,\psi_0}=-\frac{2a\eta_{12}}{\pi\eta}-\frac{2}{\pi\eta}\left[\left(\eta_{22}-\frac{\eta_{12}^2}{\eta_{11}}\right)\phi_0+\left(\eta_{32}-\frac{\eta_{12}\eta_{31}}{\eta_{11}}\right)\psi_0\right]\frac{2}{\pi\cot\beta}.$$

Thus, strictly speaking, the matrix **G** is not a generalized indentation stiffness matrix, neither the matrix **C** for a conical indenter, according to the definition by Yang (2008). Nevertheless, we can still obtain the particular physical meanings of other elements in matrix **G**. For example, we can find $(\delta Q/\delta h)|_{\phi_0=0,\psi_0=0}=2G_{21}$. Thus, under the condition of $\phi_0=\psi_0=0$, the element G_{21} still corresponds to the commonly defined indentation coefficient except for a factor 2. In the following, for simplicity, we therefore will treat the matrix **G** as a measure of related indentation coefficients as well. On the other hand, it may be inappropriate to simply treat the matrix **C** as the indentation stiffness matrix since the contact radius a also depends on the material properties of the half-space.

The indentation depth is

$$h=\frac{\pi a}{2}\cot\beta-\frac{\eta_{21}\phi_0+\eta_{31}\psi_0}{\eta_{11}}, \tag{26}$$

where a is determined from Eq. (24) as[1]

$$a=\sqrt{\frac{2\eta P}{\eta_{11}\cot\beta}}, \tag{27}$$

which indicates that the contact radius is solely determined by the total mechanical force, independent of the electric and magnetic potentials. As shown in Appendix C, the relation (26) comes from the requirement that there is no singularity in the total stress field at $r=a$, as is also the case in the elastic contact mechanics (Sneddon, 1965; Fabrikant, 1989). When $\phi_0=\psi_0=0$, we obtain $h=\pi a\cot\beta/2$, the same as that in Chen et al. (1999) and Karapetian et al. (2005) for the corresponding piezoelectric material and in Hanson (1992a) for the elastic material.

The complete and exact 3D expressions for the MEE field in the half-space due to a conical indenter are also presented in Appendix D.

[1] For stable materials, we usually have $\eta_{11}/\eta>0$. This can be readily understood from the physical consideration that a pressure P will lead to contact since no exclusive force is accounted in the present analysis. This is confirmed by the numerical calculation as presented in Section 4.

3.2.3. Spherical indenter

The pressure, normal electric displacement, and normal magnetic flux distributions under the spherical indenter are

$$p_j(r)=\frac{2\eta_{1j}}{\pi^2\eta R}\sqrt{a^2-r^2}+\frac{\eta_{1j}(h-a^2/R)+\eta_{2j}\phi_0+\eta_{3j}\psi_0}{\pi^2\eta}\frac{1}{\sqrt{a^2-r^2}}\quad (j=1,2,3). \tag{28}$$

Unlike the flat or conical indenter, there is no singularity in the total stress field either at the edge $r=a$ or the center $r=0$ of the contact area.

The resultant indentation force, total electric charge, and total magnetic flux are

$$P_j=\frac{2a}{\pi\eta}\left[\frac{2}{3}\eta_{1j}h+\left(\eta_{2j}-\frac{\eta_{1j}\eta_{21}}{3\eta_{11}}\right)\phi_0+\left(\eta_{3j}-\frac{\eta_{1j}\eta_{31}}{3\eta_{11}}\right)\psi_0\right]\quad (j=1,2,3), \tag{29}$$

or in the form of Eq. (20), the matrix $\mathbf{C}$ now reads as

$$\mathbf{C}=\frac{1}{\eta}\begin{bmatrix}\frac{2}{3}\eta_{11} & \frac{2}{3}\eta_{12} & \frac{2}{3}\eta_{13}\\ -\frac{2}{3}\eta_{12} & \frac{\eta_{12}^2}{3\eta_{11}}-\eta_{22} & \frac{\eta_{12}\eta_{13}}{3\eta_{11}}-\eta_{23}\\ -\frac{2}{3}\eta_{13} & \frac{\eta_{12}\eta_{13}}{3\eta_{11}}-\eta_{23} & \frac{\eta_{13}^2}{3\eta_{11}}-\eta_{33}\end{bmatrix}. \tag{30}$$

Again, the relation (29) is similar to that in Karapetian et al. (2005) for a piezoelectric half-space, but it cannot be reduced to that due to the different assumptions employed.

The indentation depth is

$$h=\frac{a^2}{R}-\frac{\eta_{21}\phi_0+\eta_{31}\psi_0}{\eta_{11}}, \tag{31}$$

where a is determined from Eq. (29) for $j=1$ as follows:

$$a=\sqrt[3]{\frac{3\pi\eta RP}{4\eta_{11}}}. \tag{32}$$

It is noted that relation (31) also comes from the requirement of no singularity in the total stress field at $r=a$, as shown in Appendix C.

The complete and exact 3D expressions for the MEE field in the half-space due to a spherical indenter are given in Appendix D.

3.3. Solution for electrically conducting and magnetically insulating indenters

Second, we assume that the indenter is electrically conducting but magnetically insulating. From Eq. (14), we can obtain

$$w_k(r,\theta,\ 0)=\sum_{j=1}^{2}\xi_{kj}\int_0^{2\pi}\int_0^a\frac{p_j(\rho,\theta_0)}{R_0}\rho d\rho d\theta_0\quad (k=1,2,3). \tag{33}$$

Then from the first two equations of (33), we obtain

$$\int_0^{2\pi}\int_0^a\frac{p_1(\rho,\theta_0)}{R_0}\rho\, d\rho\, d\theta_0=\frac{1}{\eta_{33}}\left[\xi_{22}w_1(r,\theta,0)-\xi_{12}w_2(r,\theta,0)\right], \tag{34a}$$

$$\int_0^{2\pi}\int_0^a\frac{p_2(\rho,\theta_0)}{R_0}\rho\, d\rho\, d\theta_0=\frac{1}{\eta_{33}}\left[-\xi_{21}w_1(r,\theta,0)+\xi_{11}w_2(r,\theta,0)\right]. \tag{34b}$$

Obviously, the above two integral equations have the same structure as those in Eq. (16), and hence exact solutions for the three common types of indenters can be derived following a similar procedure. On the other hand, the magnetic potential can be obtained from the third in Eq. (33) without solving any integral equation as

$$w_3(r,\theta,\ 0)=-\frac{1}{\eta_{33}}\left[\eta_{13}w_1(r,\theta,\ 0)+\eta_{23}w_2(r,\theta,\ 0)\right]\quad (0\le r\le a). \tag{35}$$

This solution can also be obtained directly from Eq. (16) for $j=3$ and $p_3=0$.

3.3.1. Flat indenter

The pressure and normal electric displacement distributions under the flat indenter are

$$p_1(r)=\frac{\xi_{22}h-\xi_{12}\phi_0}{\pi^2\eta_{33}}\frac{1}{\sqrt{a^2-r^2}},\quad p_2(r)=\frac{-\xi_{21}h+\xi_{11}\phi_0}{\pi^2\eta_{33}}\frac{1}{\sqrt{a^2-r^2}}. \tag{36}$$

Therefore, the resultant indentation force and total electric charge are

$$P_1 = \frac{2a(\xi_{22}h - \xi_{12}\phi_0)}{\pi\eta_{33}}, \quad P_2 = \frac{2a(-\xi_{21}h + \xi_{11}\phi_0)}{\pi\eta_{33}}, \tag{37}$$

or in the form of Eq. (20), with matrix **C** as

$$\mathbf{C} = \frac{1}{\eta_{33}}\begin{bmatrix} \xi_{22} & -\xi_{12} & 0 \\ \xi_{12} & -\xi_{11} & 0 \\ 0 & 0 & 0 \end{bmatrix}, \tag{38}$$

where we have added a null row and column so that the form of Eq. (20) keeps unchanged.

The indentation depth is

$$h = \frac{1}{\xi_{22}}\left(\frac{\pi\eta_{33}P}{2a} + \xi_{12}\phi_0\right), \tag{39}$$

and the magnetic potential distribution under the flat indenter is

$$w_3(r,\theta,\ 0) = -\frac{1}{\eta_{33}}(\eta_{13}h + \eta_{23}\phi_0), \tag{40}$$

where h is given by Eq. (39).

Similarly, the complete and exact 3D expressions for the MEE field in the half-space are presented in Appendix D.

3.3.2. Conical indenter

The pressure and normal electric displacement distributions under the conical indenter are:

$$p_1(r) = \frac{\xi_{22}\cot\beta}{2\pi\eta_{33}}\cosh^{-1}\left(\frac{a}{r}\right), \tag{41a}$$

$$p_2(r) = -\frac{\xi_{21}\cot\beta}{2\pi\eta_{33}}\cosh^{-1}\left(\frac{a}{r}\right) + \frac{(\xi_{11} - \xi_{12}^2/\xi_{22})\phi_0}{\pi^2\eta_{33}}\frac{1}{\sqrt{a^2 - r^2}}. \tag{41b}$$

The resultant indentation force and total electric charge are

$$P_1 = \frac{\xi_{22}a^2\cot\beta}{2\eta_{33}}, \quad P_2 = -\frac{\xi_{21}a^2\cot\beta}{2\eta_{33}} + \frac{2a(\xi_{11} - \xi_{12}^2/\xi_{22})\phi_0}{\pi\eta_{33}}, \tag{42}$$

or in the form of Eq. (20), but with the matrix **C** being

$$\mathbf{C} = \frac{1}{\eta_{33}}\begin{bmatrix} \frac{1}{2}\xi_{22} & -\frac{1}{2}\xi_{12} & 0 \\ \frac{1}{2}\xi_{12} & \frac{1}{2}\frac{\xi_{12}^2}{\xi_{22}} - \xi_{11} & 0 \\ 0 & 0 & 0 \end{bmatrix}. \tag{43}$$

The indentation depth is

$$h = \frac{\pi a}{2}\cot\beta + \frac{\xi_{12}}{\xi_{22}}\phi_0, \tag{44}$$

with

$$a = \sqrt{\frac{2\eta_{33}P}{\xi_{22}\cot\beta}} \tag{45}$$

which is an immediate result of the first equation in Eq. (42).

The magnetic potential distribution under the conical indenter is

$$w_3(r,\theta,\ 0) = -\frac{1}{\eta_{33}}\left[\eta_{13}(h - r\cot\beta) + \eta_{23}\phi_0\right] \quad (0 \le r \le a), \tag{46}$$

where h is given by Eq. (44).

3.3.3. Spherical indenter

The pressure and normal electric displacement distributions under the spherical indenter are

$$p_1(r) = \frac{2\xi_{22}}{\pi^2\eta_{33}R}\sqrt{a^2 - r^2}, \tag{47a}$$

$$p_2(r) = -\frac{2\xi_{21}}{\pi^2\eta_{33}R}\sqrt{a^2-r^2} + \frac{(\xi_{11}-\xi_{12}^2/\xi_{22})\phi_0}{\pi^2\eta_{33}}\frac{1}{\sqrt{a^2-r^2}}. \tag{47b}$$

The resultant indentation force and total electric charge are

$$P_1 = \frac{4\xi_{22}a^3}{3\pi\eta_{33}R}, \quad P_2 = -\frac{4\xi_{21}a^3}{3\pi\eta_{33}R} + \frac{2a(\xi_{11}-\xi_{12}^2/\xi_{22})\phi_0}{\pi\eta_{33}}, \tag{48}$$

or simply in the form of Eq. (20), with matrix **C** being

$$\mathbf{C} = \frac{1}{\eta_{33}}\begin{bmatrix} \frac{2}{3}\xi_{22} & -\frac{2}{3}\xi_{12} & 0 \\ \frac{2}{3}\xi_{12} & \frac{\xi_{12}^2}{3\xi_{22}}-\xi_{11} & 0 \\ 0 & 0 & 0 \end{bmatrix}. \tag{49}$$

The indentation depth is given by

$$h = \frac{a^2}{R} + \frac{\xi_{12}}{\xi_{22}}\phi_0, \tag{50}$$

where the contact radius a is determined from Eq. (47a) as

$$a = \sqrt[3]{\frac{3\pi\eta_{33}RP}{4\xi_{22}}} \tag{51}$$

The magnetic potential distribution under the spherical indenter is

$$w_3(r,\theta,\ 0) = -\frac{1}{\eta_{33}}\left[\eta_{13}\left(h-\frac{r^2}{2R}\right)+\eta_{23}\phi_0\right] \quad (0 \le r \le a). \tag{52}$$

3.4. Magnetically conducting and electrically insulating indenters

If the indenter is magnetically conducting but electrically insulating, then the analysis is very similar to that just described above and hence is omitted here. More specifically, to find the solutions for this case, one needs only simply to interchange the electric (magnetic) and magnetic (electric) quantities in the solutions given in Section 3.3.

3.5. Electrically and magnetically insulating indenters

We now assume that the indenter is both electrically and magnetically insulating. From Eq. (14), we obtain

$$w_k(r,\theta,\ 0) = \xi_{k1}\int_0^{2\pi}\int_0^a \frac{p_1(\rho,\theta_0)}{R_0}\rho\, d\rho\, d\theta_0 \quad (k=1,2,3). \tag{53}$$

When $k=1$, the above equation gives

$$\int_0^{2\pi}\int_0^a \frac{p_1(\rho,\theta_0)}{R_0}\rho\, d\rho\, d\theta_0 = \frac{1}{\xi_{11}}w_1(r,\theta,0). \tag{54}$$

The exact solutions for the three common types of indenters then can be readily obtained by using the results of Fabrikant (1989, 1991) and Hanson (1992a,b). The electric and magnetic potentials can be obtained from Eq. (53) as

$$w_k(r,\theta,0) = \frac{\xi_{k1}}{\xi_{11}}w_1(r,\theta,0) \quad (k=2,3; \quad 0 \le r \le a). \tag{55}$$

3.5.1. Flat indenter

The pressure distribution under the indenter is

$$p_1(r) = \frac{h}{\pi^2\xi_{11}}\frac{1}{\sqrt{a^2-r^2}}. \tag{56}$$

The resultant indentation force is

$$P_1 = \frac{2ah}{\pi\xi_{11}}, \tag{57}$$

which can also be written in the form of Eq. (20), with the matrix **C** being

$$\mathbf{C} = \frac{1}{\xi_{11}}\begin{bmatrix} 1 & 0 & 0 \\ 0 & 0 & 0 \\ 0 & 0 & 0 \end{bmatrix}. \tag{58}$$

The indentation depth is

$$h = \frac{\pi \xi_{11} P}{2a}. \tag{59}$$

The electric and magnetic potentials under the indenter are

$$w_k(r,\theta,0) = \frac{\xi_{k1}}{\xi_{11}} h, \quad (k = 2,3; \quad 0 \le r \le a). \tag{60}$$

The complete and exact 3D expressions for the MEE field in the half-space under this boundary condition are presented in Appendix D.

3.5.2. Conical indenter

The pressure distribution under the indenter is

$$p_1(r) = \frac{\cot\beta}{2\pi\xi_{11}} \cosh^{-1}\left(\frac{a}{r}\right). \tag{61}$$

The resultant indentation force is

$$P_1 = \frac{a^2 \cot\beta}{2\xi_{11}}, \tag{62}$$

which can be rewritten in the form of Eq. (20), but with the matrix **C** being

$$\mathbf{C} = \frac{1}{2\xi_{11}} \begin{bmatrix} 1 & 0 & 0 \\ 0 & 0 & 0 \\ 0 & 0 & 0 \end{bmatrix}. \tag{63}$$

The indentation depth is

$$h = \frac{\pi}{2} a \cot\beta, \tag{64}$$

where the contact radius is given by

$$a = \sqrt{\frac{2\xi_{11} P}{\cot\beta}}. \tag{65}$$

The electric and magnetic potentials under the indenter are

$$w_k(r,\theta,0) = \frac{\xi_{k1}}{\xi_{11}} (h - r\cot\beta) \quad (k = 2,3; \quad 0 \le r \le a). \tag{66}$$

3.5.3. Spherical indenter

The pressure distribution under the spherical indenter is

$$p_1(r) = \frac{2}{\pi^2 \xi_{11} R} \sqrt{a^2 - r^2}. \tag{67}$$

The resultant indentation force is

$$P_1 = \frac{4a^3}{3\pi\xi_{11} R}, \tag{68}$$

which, when expressed in the form of Eq. (20), has the matrix **C** as

$$\mathbf{C} = \frac{2}{3\xi_{11}} \begin{bmatrix} 1 & 0 & 0 \\ 0 & 0 & 0 \\ 0 & 0 & 0 \end{bmatrix}. \tag{69}$$

The indentation depth is

$$h = \frac{a^2}{R}, \tag{70}$$

where the contact radius a is determined from Eq. (68) as

$$a = \sqrt[3]{\frac{3\pi\xi_{11} RP}{4}}. \tag{71}$$

The electric and magnetic potentials under the indenter are

$$w_k(r,\theta,0) = \frac{\xi_{k1}}{\xi_{11}} \left(h - \frac{r^2}{2R}\right) \quad (k = 2,3; \quad 0 \le r \le a). \tag{72}$$

4. Numerical results and discussion

A complete set of material properties of single-phase multiferroic materials (such as Cr_2O_3, $BiFeO_3$, $YMnO_3$, $LuFe_2O_3$, etc.) cannot be found in literature. Hence, we confine ourselves to the MEE composite materials made of piezoelectric and magnetostrictive phases. The material properties of piezoelectric ceramic $BaTiO_3$ and those of piezomagnetic crystalline $CoFe_2O_4$ are chosen for the following numerical illustrations, and they are given in Tables 1 and 2, where all the absent material constants equal zero. It then becomes obvious that, there is no direct ME effect in either phase, but the composite does exhibit the ME coupling due to the so-called product property of the composite through the mechanical strain interaction.

The material properties of the composite are estimated using the simple rule of mixture according to the volume fractions (Sih and Chen, 2003). Denoting for the composite the volume fraction of $CoFe_2O_4$ as x, and that of $BaTiO_3$ as $1-x$, we then have

$$M_C = M_E(1-x) + M_M x, \tag{73}$$

where M represents an arbitrary material constant, and the subscripts C, E, and M indicate the composite, piezoelectric phase and piezomagnetic phase, respectively.

In the following, we consider five different cases of material combinations, by taking the volume fraction of $CoFe_2O_4$ as $x=0$, 0.25, 0.5, 0.75, and 1, respectively. Obviously, when $x=0$, the composite is purely piezoelectric, whilst $x=1$ corresponds to a purely piezomagnetic material. Various degeneration cases are discussed in Appendix E. Among many different combinations of material constants appearing in matrices **C** and **G**, which vary with the geometry and magnetoelectric property of the indenter, ξ_{ij} $(i,j=1,2,3)$ are the most fundamental. These and the associated parameters η_{ij}, the cofactors of $[\xi_{ij}]$ are listed in Table 3 for the five values of the volume fraction x.

Table 3 shows that the parameter ξ_{23}, which is associated with the ME effect or coupling during indentation, is not zero when $x \neq 0$. This clearly attributes to the product property of the composite which in turn is caused by the mechanical strain interaction. Thus, the indentation technique can be used to characterize the ME effect in composites or crystals. From this table, it is also seen that the two parameters ξ_{22} and ξ_{33}, which in certain sense correspond to the dielectric and magnetic properties respectively, vary with the volume fraction more significantly than the other parameters. Their variations with the volume fraction x are shown in Fig. 2. When the electric (or magnetic) field tends to decouple from the magneto-elastic (or electro-elastic) coupled field, ξ_{22} (or ξ_{33}) increases rapidly, and finally arrives at the value of $\xi_{22} = -1/(2\pi\sqrt{\varepsilon_{11}\varepsilon_{33}})$ (or $\xi_{33} = -1/(2\pi\sqrt{\mu_{11}\mu_{33}})$), see Appendix E.

4.1. Flat-ended indenter

We first assume that the flat-ended circular indenter is electrically and magnetically conducting (Case A). As discussed in Section 3, when the indenter is flat-ended, either the matrix **G** or **C** can be a direct measure of various stiffness coefficients related to the indentation process. For instance, we choose matrix **C** which can be expressed as

$$\mathbf{C} = \begin{bmatrix} 1 & 0 & 0 \\ 0 & -1 & 0 \\ 0 & 0 & -1 \end{bmatrix} \frac{1}{\eta}\left[\eta_{ij}\right] = \begin{bmatrix} 1 & 0 & 0 \\ 0 & -1 & 0 \\ 0 & 0 & -1 \end{bmatrix} [\xi_{ij}]^{-1}$$

Table 1
Material coefficients of the piezoelectric $BaTiO_3$ (Pan, 2001). (c_{ij} in 10^9 N/m^2, e_{ij} in C/m^2, ε_{ij} in 10^{-9} C^2/(N m^2), μ_{ij} in 10^{-6} N s^2/C^2).

c_{11}	c_{12}	c_{13}	c_{33}	c_{44}	c_{66}
166	77	78	162	43	44.5
e_{31}	e_{33}	e_{15}			
−4.4	18.6	11.6			
ε_{11}	ε_{33}		μ_{11}	μ_{33}	
11.2	12.6		5	10	

Table 2
Material coefficients of the magnetostrictive $CoFe_2O_4$ (Pan, 2001). (c_{ij} in 10^9 N/m^2, q_{ij} in N/(A m), ε_{ij} in 10^{-9} C^2/(N m^2), μ_{ij} in 10^{-6} N s^2/C^2).

c_{11}	c_{12}	c_{13}	c_{33}	c_{44}	c_{66}
286	173	170.5	269.5	45.3	56.5
q_{31}	q_{33}	q_{15}			
580.3	699.7	550			
ε_{11}	ε_{33}		μ_{11}	μ_{33}	
0.08	0.093		590	157	

Table 3
Basic indentation parameters for different material combinations.[a]

volume fraction x	$[\xi_{ij}]$	$\eta=\lvert\xi_{ij}\rvert$[b]	$[\eta_{ij}]$
0.00	$\begin{bmatrix} 2.16825 & 1.76207 & 0 \\ & -1.04710 & 0 \\ \text{sym.} & & -22.5079 \end{bmatrix}$	−2.58086	–
0.25	$\begin{bmatrix} 2.08613 & 1.76439 & 1.95380 \\ & -1.48486 & 2.71289 \\ \text{sym.} & & -1.88746 \end{bmatrix}$	6.44020	$\begin{bmatrix} 2.80188 & 3.33553 & 3.37978 \\ & -3.94131 & -2.21216 \\ \text{sym.} & & -0.340891 \end{bmatrix}$
0.50	$\begin{bmatrix} 2.03552 & 1.77480 & 1.93900 \\ & -2.35928 & 2.85507 \\ \text{sym.} & & -1.00418 \end{bmatrix}$	5.14794	$\begin{bmatrix} 2.36834 & 1.78776 & 5.08136 \\ & -2.04779 & -2.37022 \\ \text{sym.} & & -0.511736 \end{bmatrix}$
0.75	$\begin{bmatrix} 2.00607 & 1.77755 & 1.89271 \\ & -4.94527 & 2.89808 \\ \text{sym.} & & -0.683397 \end{bmatrix}$	7.01360	$\begin{bmatrix} 3.37875 & 1.22026 & 9.87511 \\ & -1.37452 & -2.44936 \\ \text{sym.} & & -1.02365 \end{bmatrix}$
1.00	$\begin{bmatrix} 1.98978 & 0 & 1.85696 \\ & -184.516 & 0 \\ \text{sym.} & & -0.517441 \end{bmatrix}$	−1.03304	–

[a] Units: ξ_{11} in 10^{-12} m^2/N, ξ_{12} in 10^{-3} m^2/C, ξ_{13} in 10^{-6} mA/N, ξ_{22} in 10^7 N m^2/C^2, ξ_{23} in 10^3 V A/N, ξ_{33} in 10^3 A^2/N; η in 10^{-2} m^4 A^2/(N C^2); η_{11} in 10^{10} m^2 A^2/C^2, η_{12} in m^2 A^2/(C N), η_{13} in 10^1 m^3 A/C^2, η_{22} in 10^{-9} m^2 A^2/N^2, η_{23} in 10^{-9} m^3 A/(N C), η_{33} in 10^{-4} m^4/C^2.
[b] For volume fraction x=0 of $CoFe_2O_4$, $\eta=\lvert\xi_{ij}\rvert$ (i,=1,2), the unit is 10^{-5} m^4/C^2; and for x=1, $\eta=\lvert\xi_{ij}\rvert$ (i, j=1, 3), the unit is 10^{-9} m^2 A^2/N^2.

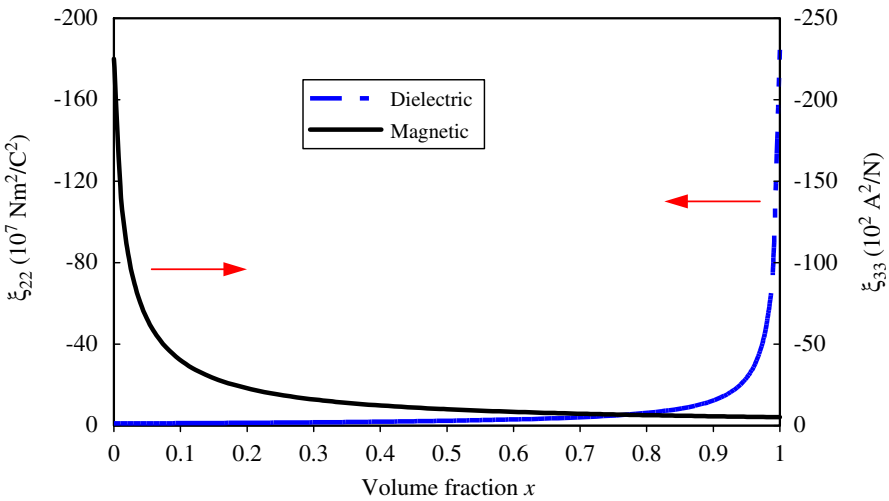

Fig. 2. Variation of ξ_{22} and ξ_{33} with volume fraction x of $CoFe_2O_4$.

Hence, one can easily compute matrix **C** once matrix $[\xi_{ij}]$ is calculated. Table 4 lists the algebraic values of matrix **C** for the five different material combinations.

It is observed from Table 4, the indentation elastic stiffness C_{11} increases with the volume fraction x. This is consistent with the fact that the piezomagnetic phase $CoFe_2O_4$ is stiffer than the piezoelectric phase $BaTiO_3$. Also as expected, with increasing x, the indentation piezoelectric coefficient C_{12} decreases but the indentation piezomagnetic coefficients C_{13} increases. However, no monotonic variation of the indentation ME coefficient C_{23} can be observed. The complete spectrum of its variation with the volume fraction is shown in Fig. 3, which indicates that the indentation ME coefficient C_{23} arrives at its maximum around x=0.5. This is physically reasonable as both phases play a somewhat equal role at such a volume fraction and the mechanical strain interaction between the two phases is optimized (Petrov and Srinivasan, 2008; Pan and Wang, 2009).

For comparison, the values of the matrix **C** for other three cases, (i.e. Case B: electrically conducting and magnetically insulating, Case C: electrically insulating and magnetically conducting, and Case D: electrically and magnetically insulating), are summarized in Table 5. It should be noted that for Case D, although the only non-zero element in matrix **C** is C_{11}, it is not identical to the elastic case. To make such a comparison, we denote Case E as the purely elastic case where the elastic field is fully decoupled from the electric and magnetic fields. Then, we can calculate according to Fabrikant (1989)

$$\textit{Case}\ \mathrm{E}:\ C_{11}=3.96226,\ 4.25823,\ 4.52352,\ 4.76784,\ 4.99705(10^{11}\,\mathrm{N/m^2})$$

Table 4
Matrix **C** for an electrically and magnetically conducting flat-ended indenter.[a]

Volume fraction x	**C**	Volume fraction x	**C**
0.00	$\begin{bmatrix} 4.05716 & 6.82744 & 0 \\ -6.82744 & 8.40128 & 0 \\ 0 & 0 & 0.444288 \end{bmatrix}$	0.75	$\begin{bmatrix} 4.81742 & 1.73985 & 14.0799 \\ -1.73985 & 1.95980 & 3.49230 \\ -14.0799 & 3.49230 & 14.5953 \end{bmatrix}$
0.25	$\begin{bmatrix} 4.35061 & 5.17923 & 5.24794 \\ -5.17923 & 6.11985 & 3.43493 \\ -5.24794 & 3.43493 & 5.29318 \end{bmatrix}$	1.00	$\begin{bmatrix} 5.00890 & 0 & 17.9756 \\ 0 & 0.0541958 & 0 \\ -17.9756 & 0 & 19.2614 \end{bmatrix}$
0.50	$\begin{bmatrix} 4.60055 & 3.47276 & 9.87067 \\ -3.47276 & 3.97789 & 4.60422 \\ -9.87067 & 4.60422 & 9.94060 \end{bmatrix}$		

[a] Units: C_{11} in 10^{11} N/m^2, C_{12}, C_{21} in 10^1 C/m^2, C_{13}, C_{31} in 10^2 N/(mA), C_{22} in 10^{-8} C^2/(N m^2), C_{23}, C_{32} in10^{-8} N/(V A), C_{33} in 10^{-4} N/A^2.

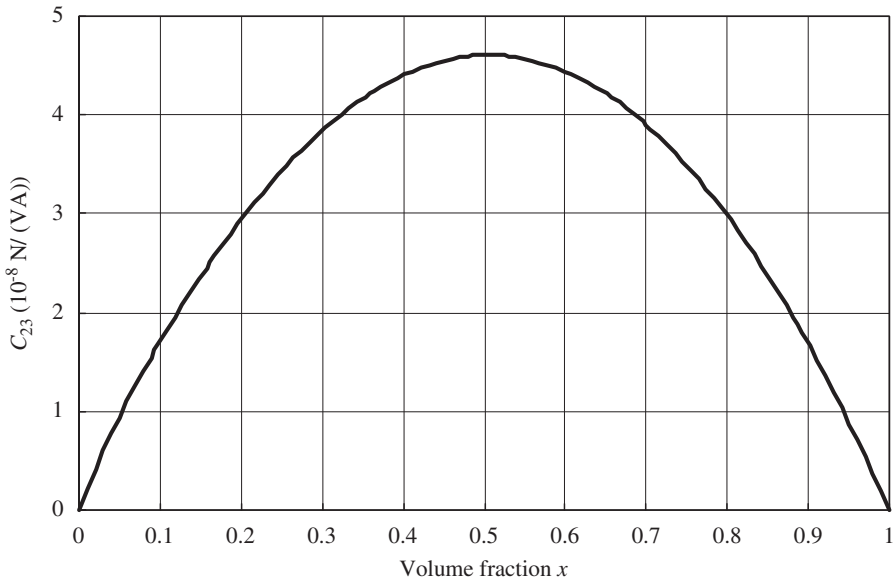

Fig. 3. Variation of the indentation ME coefficient with volume fraction x.

for x=0, 0.25, 0.50, 0.75 and 1.00, respectively. Therefore, we observe that the indentation stiffness C_{11} varies with the electromagnetic properties of the indenter, and in general for $x \neq 0$, we have

$$\text{Case D} > \text{Case C} > \text{Case B} > \text{Case A} > \text{Case E}$$

In other words, among the five cases, the purely elastic case has the smallest C_{11}! When the elastic field in the material couples with the electric or magnetic field, the well-known piezoelectric (or piezomagnetic) stiffening effect plays an important role. The stiffening effect is more obvious when the indenter is electrically (or magnetically) insulating than when it is electrically (or magnetically) conducting.

When x=0, the magnetic field in the material decouples from the coupled electro-elastic field. In this case, the magnetically insulating indenter will lead to a null magnetic field in the half-space, and exerts no effect on the electro-elastic field. Similarly, when x=1, for which the electric field becomes independent of the coupled magneto-elastic field in the half-space, a change in the electric property of the indenter does not affect the magneto-elastic field.

The relative difference of the indentation stiffness coefficient C_{11} between Case D and Case E, defined as RD=(Case D − Case E)/Case E, can be calculated as

$$\text{RD} = 16.40\%,\ 12.57\%,\ 8.60\%,\ 4.55\% \text{ and } 2.86\%$$

for x=0, 0.25, 0.50, 0.75 and 1.00, respectively. It is seen that for the pure piezoelectric material $BaTiO_3$ (x=0), the difference between the (piezoelectric) coupled theory and the elastic theory is significant, and the coupled theory should be utilized to interpret the indentation results. For the pure piezomagnetic material $CoFe_2O_4$ (x=1), the difference by using the elastic theory is around 3%. Thus, the feasibility of using the relatively simple elasticity theory to characterize the material properties of piezoelectric, piezomagnetic or multiferroic materials depends significantly on the coupling among various fields in the materials. Simulations based on the completely coupled theory should be performed to evaluate the accuracy of various simplified models.

Table 5
Matrix **C** for a flat-ended indenter under different electric and magnetic boundary conditions over the MEE half-space composite with different volume fraction x.[a]

Volume fraction x	**C**		
	Case B: Electrically conducting, magnetically insulating	*Case C:* Electrically insulating, magnetically conducting	*Case D:* Electrically and magnetically insulating
0.00	$\begin{bmatrix} 4.05716 & 6.82744 & 0 \\ -6.82744 & 8.40128 & 0 \\ 0 & 0 & 0 \end{bmatrix}$	$\begin{bmatrix} 4.61201 & 0 & 0 \\ 0 & 0 & 0 \\ 0 & 0 & 0.444288 \end{bmatrix}$	$\begin{bmatrix} 4.61201 & 0 & 0 \\ 0 & 0 & 0 \\ 0 & 0 & 0 \end{bmatrix}$
0.25	$\begin{bmatrix} 4.35581 & 5.17583 & 0 \\ -5.17583 & 6.11963 & 0 \\ 0 & 0 & 0 \end{bmatrix}$	$\begin{bmatrix} 4.78892 & 0 & 4.95724 \\ 0 & 0 & 0 \\ -4.95724 & 0 & 5.29298 \end{bmatrix}$	$\begin{bmatrix} 4.79357 & 0 & 0 \\ 0 & 0 & 0 \\ 0 & 0 & 0 \end{bmatrix}$
0.50	$\begin{bmatrix} 4.61035 & 3.46819 & 0 \\ -3.46819 & 3.97768 & 0 \\ 0 & 0 & 0 \end{bmatrix}$	$\begin{bmatrix} 4.90373 & 0 & 9.46872 \\ 0 & 0 & 0 \\ -9.46872 & 0 & 9.94007 \end{bmatrix}$	$\begin{bmatrix} 4.91275 & 0 & 0 \\ 0 & 0 & 0 \\ 0 & 0 & 0 \end{bmatrix}$
0.75	$\begin{bmatrix} 4.83100 & 1.73648 & 0 \\ -1.73648 & 1.95972 & 0 \\ 0 & 0 & 0 \end{bmatrix}$	$\begin{bmatrix} 4.97188 & 0 & 13.7699 \\ 0 & 0 & 0 \\ -13.7699 & 0 & 14.5946 \end{bmatrix}$	$\begin{bmatrix} 4.98487 & 0 & 0 \\ 0 & 0 & 0 \\ 0 & 0 & 0 \end{bmatrix}$
1.00	$\begin{bmatrix} 5.02568 & 0 & 0 \\ 0 & 0.0541958 & 0 \\ 0 & 0 & 0 \end{bmatrix}$	$\begin{bmatrix} 5.00890 & 0 & 17.9756 \\ 0 & 0 & 0 \\ -17.9756 & 0 & 19.2614 \end{bmatrix}$	$\begin{bmatrix} 5.02568 & 0 & 0 \\ 0 & 0 & 0 \\ 0 & 0 & 0 \end{bmatrix}$

[a] Units: C_{11} in 10^{11} N/m^2, C_{12}, C_{21} in 10^1 C/m^2, C_{13}, C_{31} in 10^2 N/(mA), C_{22} in 10^{-8} C^2/(N m^2), C_{23}, C_{32} in 10^{-8} N/(V A), C_{33} in 10^{-4} N/A^2.

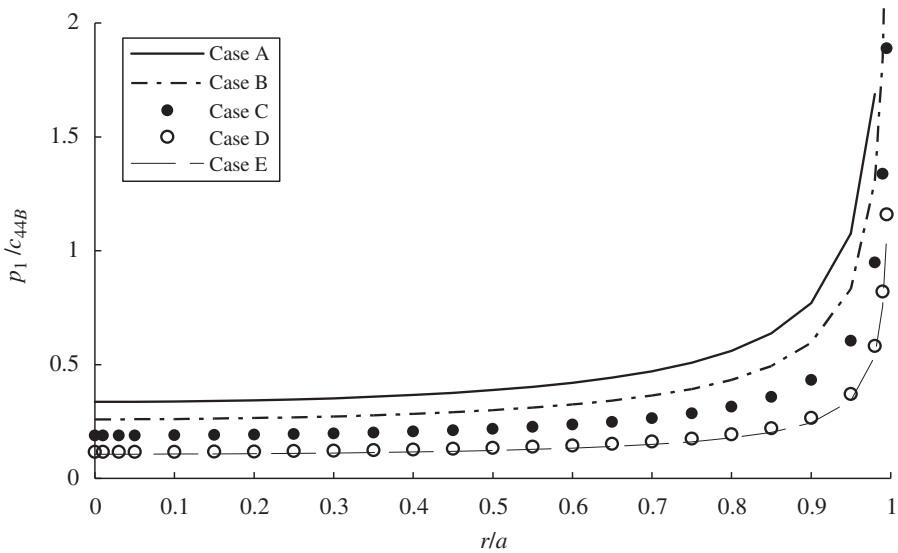

Fig. 4. Distribution of dimensionless pressure (p_1/c_{44B}) under the flat-ended indenter where h/a=0.1, $\phi_0\sqrt{\varepsilon_{33B}/c_{44B}}/a=1$, $\psi_0\sqrt{\mu_{33B}/c_{44B}}/a=0.5$. The subscript B indicates the material constant of $BaTiO_3$. The volume fraction of $CoFe_2O_4$ phase in the composite is x=0.5.

Fig. 4 shows the pressure distribution under the flat-ended indenter for the five different cases discussed. The volume fraction is fixed at x=0.5. The dimensionless mechanical penetration h/a, electric potential $\phi_0\sqrt{\varepsilon_{33B}/c_{44B}}/a$, and magnetic potential $\psi_0\sqrt{\mu_{33B}/c_{44B}}/a$ are taken to be 0.1, 1 and 0.5, respectively. For all the five cases, the pressure tends to infinity at the contact edge (r=a), exhibiting a usual square-root singularity as shown by Eq. (18), (36), or (56). It is clear that, in addition to the mechanical penetration, different electric and magnetic potentials may be applied so that the magnitude of the pressure under the indenter can be adjusted. Similar observation can also be made with regard to the electric displacement and normal magnetic flux distributions under the indenter. In fact, the magnitude of any physical field variable at a point in the multiferroic half-space can also be controlled by the mechanical, electric or magnetic means due to the coupling among the three fields. This feature will be further discussed for a spherical indenter to be considered later.

4.2. Conical indenter

With the basic material parameters of the indentation given in Table 3, one can easily obtain the matrix **C** for a conical or spherical indenter. The discussions will be similar to those for the flat-ended indenter, and hence are omitted here. Below, however, we pay our attention to other two important issues.

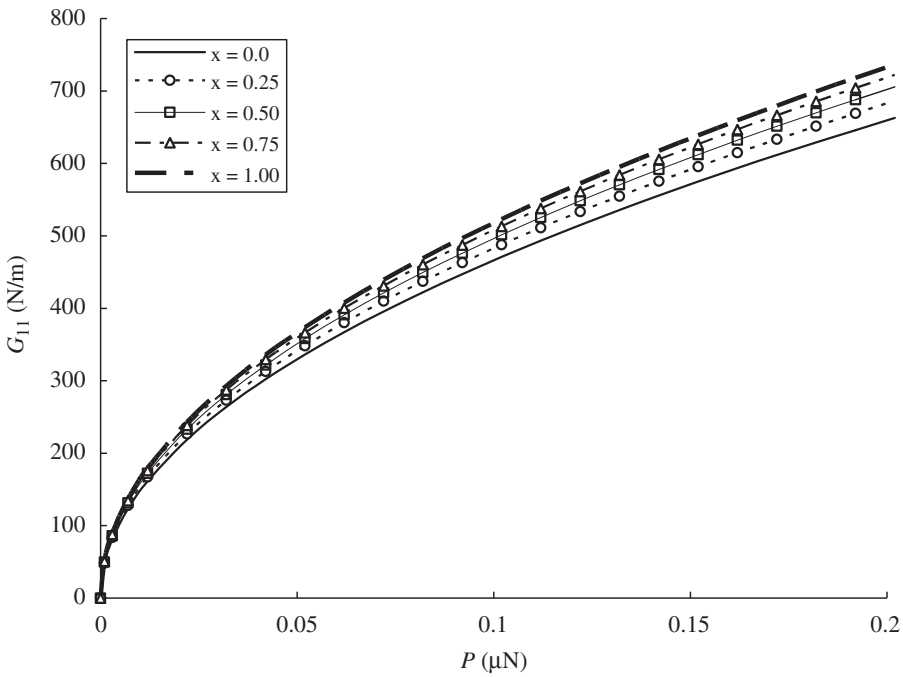

Fig. 5. G_{11} for an electrically and magnetically conducting conical indenter with β=15°.

First, let us examine the element $G_{11}=a\eta_{11}/\eta$ of the matrix **G**, which equals half of the indentation stiffness coefficient of an electrically and magnetically conducting conical indenter as shown in Section 3. The contact radius a varies with the total pressure according to Eq. (27). Thus, the indentation stiffness coefficient varies with the total pressure, as shown in Fig. 5. This is somewhat different from Kalinin et al. (2004) due to the fact that a different definition of the stiffness coefficient (Yang, 2008) has been employed here. In particular, if we take C_{11} as the indentation stiffness coefficient by following Kalinin et al. (2004), we will then obtain a constant stiffness coefficient, which could not be obtained directly from the experimental P–h curves. Comprehensive discussion also can be made on other elements of the matrix **G**, or various indentation coefficients strictly defined according to Yang (2008) and on the other conditions such as various ME properties of the indenter.

Second, let us look at the difference of the pressure distribution under the indenter caused by different conditions concerning with the vanishing stress singularity at the contact edge (r=a), see further discussions presented in Appendix C. For convenience, Condition 1 is referred to the requirement that only the mechanically induced stress is non-singular at r=a, while Condition 2 corresponds to the case where there should be no singularity in the total stress at r=a. For an electrically and magnetically conducting conical indenter, the distributions of the dimensionless pressure p_1/c_{44B} (with subscript B for the material constant of $BaTiO_3$) are shown in Fig. 6 for the two conditions when the volume fraction of $CoFe_2O_4$ phase in the multiferroic half-space equals x=0.5. When Condition 1 is used, the pressure distribution apparently depends on the applied electric and magnetic potentials, and three combinations of them are considered. As indicated in the figure, the first and second numbers in parentheses for Condition 1 are the dimensionless electric and magnetic potentials, defined by $\phi_0\sqrt{\varepsilon_{33B}/c_{44B}}/a$ and $\psi_0\sqrt{\mu_{33B}/c_{44B}}/a$, respectively. The dimensionless radial coordinate r/a is used in the figure, and it should be remembered that, unlike the flat-ended indenter, here a is not a constant, and will be different from each other for the four curves in the figure (three curves for Conditions 1 and one curve for Condition 2). Also, the penetration depth h is not specified in the figure; it actually relates to the total mechanical force as well as the electric and magnetic potentials through Eqs. (26) and (27). As can be seen from the figure, the pressure does not tend to infinity at r=a when Condition 2 is employed. Use of Condition 1, however, will induce a pressure having a square-root singularity at the contact edge, unless ϕ_0=ψ_0=0, for which the result becomes identical to that for Condition 2. Although it seems that Condition 2 is physically more reasonable than Condition 1, delicate experiments are especially desired to justify it.

4.3. Spherical indenter

For a spherical indenter, here we confine ourselves to the induced MEE field in the half-space. The exact 3D expressions are presented in Appendix D. It can be observed from there that the solutions are expressed in terms of elementary functions, thus greatly facilitating our computation as well as future applications. The calculations are performed for an electrically and magnetically conducting spherical indenter on a multiferroic half-space with the volume fraction of the piezomagnetic phase being fixed at x=0.5. Shown in Fig. 7 are the distributions of some dimensionless physical quantities along the axisymmetric

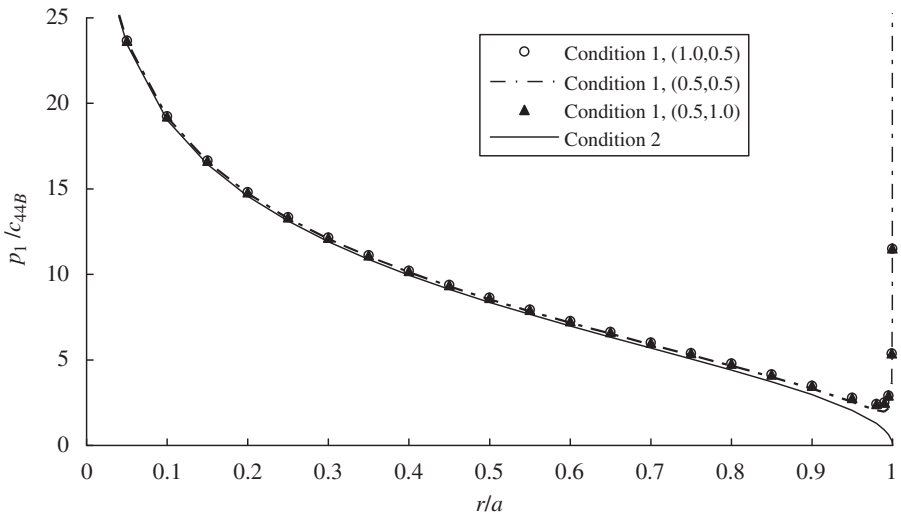

Fig. 6. Distribution of the dimensionless pressure (p_1/c_{44B}) under the electrically and magnetically conducting conical indenter with β=15° for two different conditions. The first and second numbers in parentheses for Condition 1 are the dimensionless electric and magnetic potentials, defined by $\phi_0\sqrt{\varepsilon_{33B}/c_{44B}}/a$ and $\psi_0\sqrt{\mu_{33B}/c_{44B}}/a$, respectively. The subscript B indicates the material constant of $BaTiO_3$. The volume fraction of $CoFe_2O_4$ phase in the multiferroic half-space equals 0.5.

axis z (or r=0). The total dimensionless mechanical force is specified as $P/(c_{44B}R^2)=10^{-5}$, while three combinations of the electric and magnetic potentials, (0,0), (1.0,0.5), and (0.5,1.0), are considered, both being in dimensionless form defined by $\phi_0\sqrt{\varepsilon_{33B}/c_{44B}}/R$ and $\psi_0\sqrt{\mu_{33B}/c_{44B}}/R$, respectively. All the results are obtained by using Condition 2, as noticed above. Thus, the contact radius is solely determined by the total mechanical force once the material of the half-space is specified, as seen from Eq. (32), and the mechanical penetration depth h is then determined from Eq. (31).

As shown in Fig. 7, when both the electric and magnetic potentials vanish, all the physical field variables also seem to disappear. However, this is not the case; in fact, their magnitudes are very small when compared to those for the other cases. To make it clear, we display in Figs. 8(a) and (b), respectively, the distribution of the axial displacement $u_z(0,z)/R$ and that of the normal stress $\sigma_{zz}(0,z)/c_{44B}$ for ϕ_0=ψ_0=0 only. As mentioned earlier, the results for Condition 1 and Condition 2 are the same in this particular case. Therefore, Fig. 7 illustrates that the difference of the MEE fields in the half-space between the two different conditions could be substantial, which of course depends on the magnitudes of electric and magnetic potentials applied on the indenter. For example, by comparing Fig. 7(a) with Fig. 8(a), it is seen that the vertical displacement induced by the mechanical force only is positive as expected, while when the electric and magnetic potentials are applied on the indenter and Condition 2 is used, the vertical displacement could be negative, which can also be seen from Eq. (31). Such characters may be utilized to experimentally determine what kind of condition (Condition 1, Condition 2, or other possible alternatives) should be employed in the analysis.

A common feature that can be observed from Figs. 7 and 8 is that all physical variables diminish rapidly with depth. This is identical to the physical nature of the problem, and also can be explicitly seen from the analytical solutions given in Appendix D. Of particular interest is the distribution of the normal stress component σ_{zz} in Fig. 7(d). For the two potential combinations (1.0,0.5) and (0.5,1.0), the stress first changes from a small negative value to a maximum negative value, then increases until the maximum tensile value is reached, and eventually diminishes with increasing depth. Thus, the maximum tensile stress occurs at a certain depth under the indenter. The results shown in Fig. 7(d) also indicate that the stress field in the half-space can be conveniently controlled through the electric or magnetic means or both. It is noted that, since Condition 1 is employed, σ_{zz} is the same for all the three different cases of potential combinations. This can be easily seen from Eqs. (28) and (31) that the pressure under the indenter is independent of the electric and magnetic potentials.

With regard to the distribution of the radial stress component σ_{rr} or the circumferential stress component $\sigma_{\theta\theta}$, a similar but relatively simpler variation can be seen from Fig. 7(g). Note that these two stress components are equal at r=0 which means physically there is no preferential direction and all normal stress components should be identical since the $r-\theta$ plane is a plane of isotropy for the transversely isotropic multiferroic materials considered in this paper. Their equivalence could also be verified mathematically based on the exact expressions given in Eqs. (D5) and (D8) of Appendix D, from which we obtain $\sigma_2^I=\sigma_2^{II}=0$ by carrying out the limit $r\to 0$. The maximum tensile radial (or circumferential) stress also occurs at a certain depth under the indenter, but it is closer to the surface than that for the stress component σ_{zz}. These tensile stress locations could potentially initiate a crack (it is of course also related to the fracture criterion, and actually, the maximum stress may occur at a place deviating from the axisymmetric axis, e.g. Ding et al., 2006).

From Figs. 7(b) and 7(c), we can see that the calculated electric and magnetic potentials coincide with the prescribed values at the surface. This, in certain sense, verifies our analytical solutions.

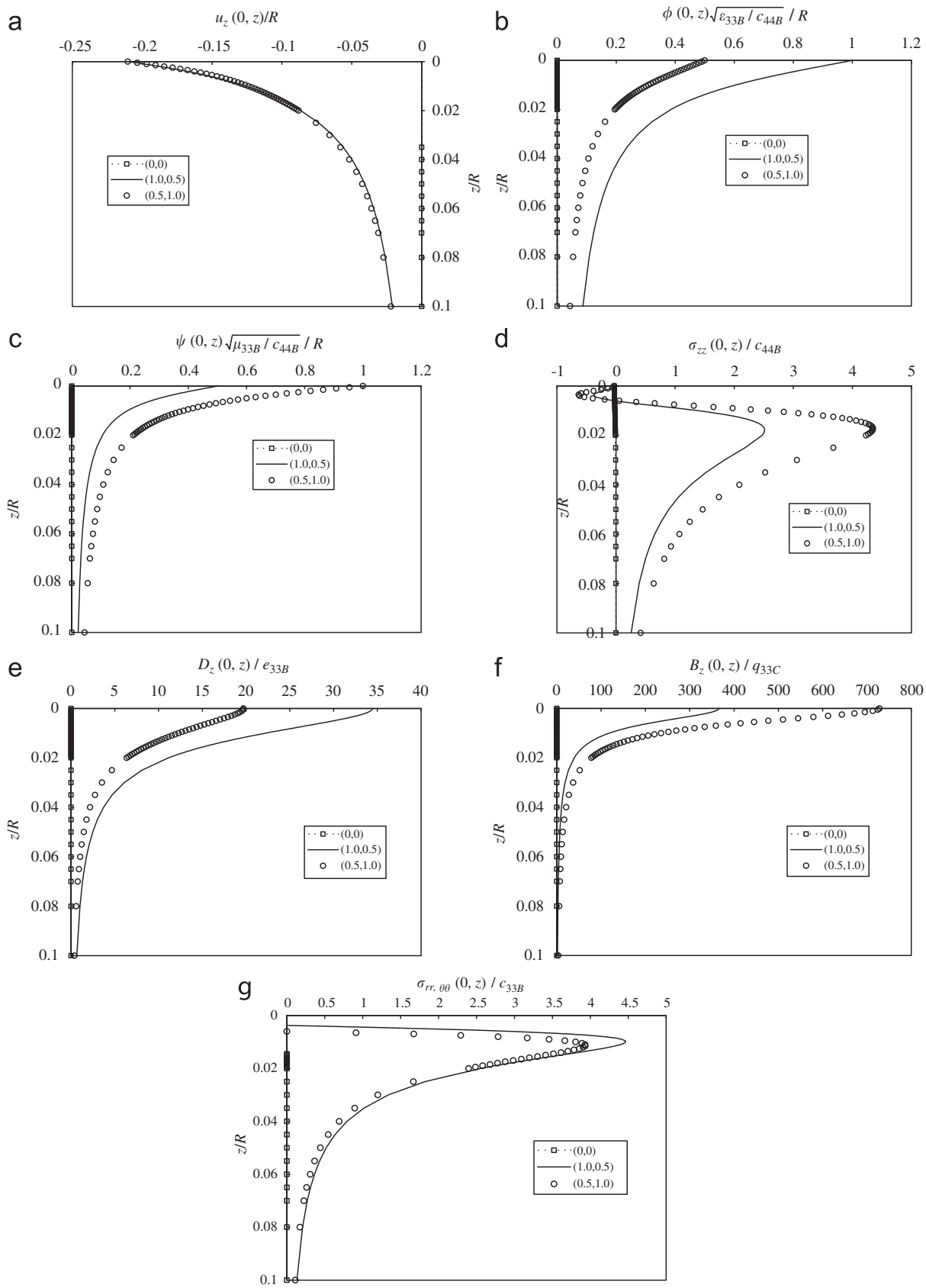

Fig. 7. Distributions of some dimensionless physical quantities along the axisymmetric axis in the multiferroic half-space ($x=0.5$) when it is pressed by an electrically and magnetically conducting spherical indenter with a prescribed total force $P/(c_{44B}R^2)=10^{-5}$: (a) $u_z(0, z)/R$, (b) $\phi(0,z)\sqrt{\varepsilon_{33B}/c_{44B}}/R$, (c) $\psi(0,z)\sqrt{\mu_{33B}/c_{44B}}/R$, (d) $\sigma_{zz}(0, z)/c_{44B}$, (e) $D_z(0, z)/e_{33B}$, (f) $B_z(0, z)/q_{33C}$, and (g) $\sigma_{rr}(0, z)/c_{44B}=\sigma_{\theta\theta}(0,z)/c_{44B}$. The first and second numbers in parentheses in the legends are the dimensionless electric and magnetic potentials, defined by $\phi_0\sqrt{\varepsilon_{33B}/c_{44B}}/R$ and $\psi_0\sqrt{\mu_{33B}/c_{44B}}/R$, respectively. The subscripts B and C indicate the material constant of $BaTiO_3$ and $CoFe_2O_4$, respectively.

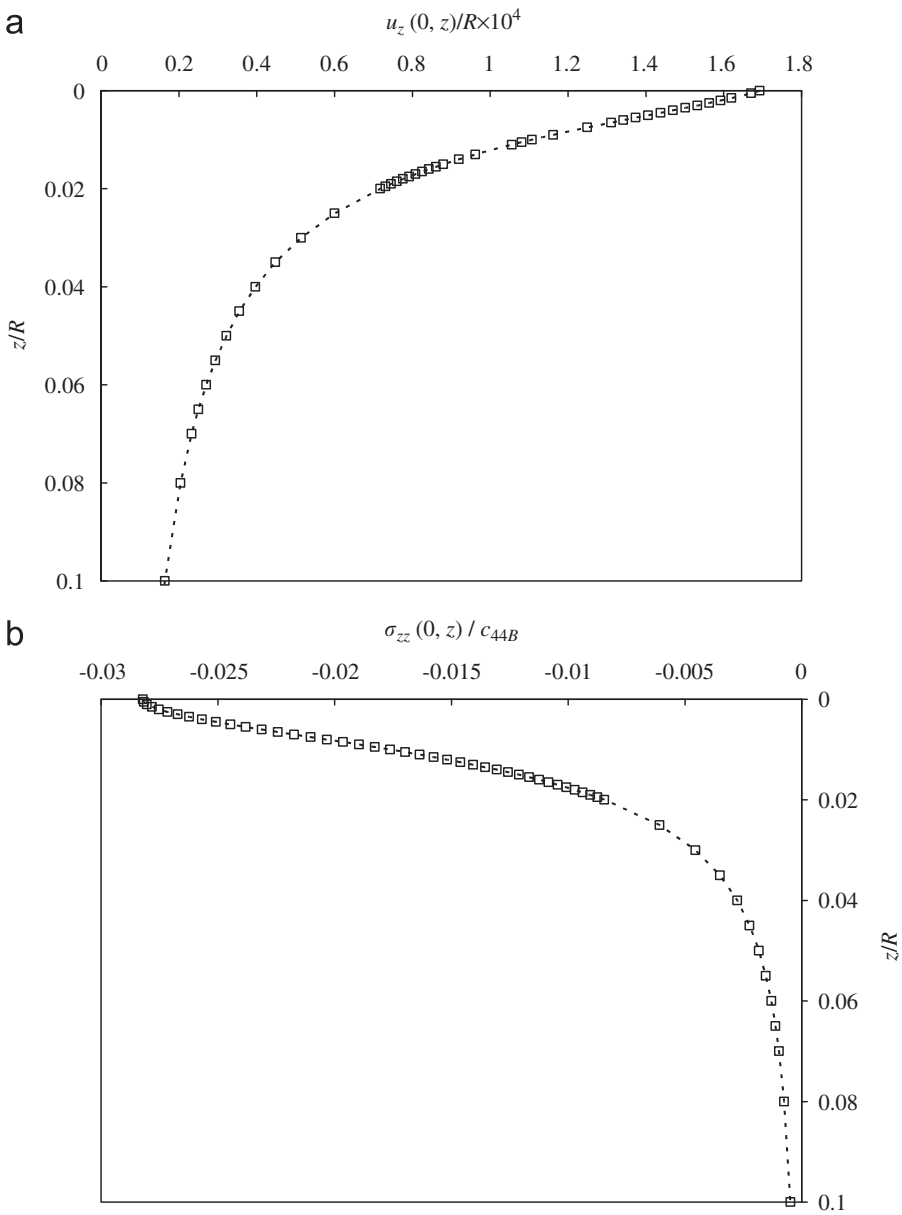

Fig. 8. Distributions of $u_z(0, z)/R$ and $\sigma_{zz}(0, z)/c_{44B}$ for $\phi_0=\psi_0=0$ with all other parameters being the same as those in Fig. 7.

5. Conclusions

In this paper, we have presented a unified fundamental theory to deal with the contact problem between a rigid punch (or indenter) and a multiferroic half-space. The indenter may have a flat-ended, conical or spherical shape, and may be electrically and magnetically conducting, electrically conducting and magnetically insulating, electrically insulating and magnetically conducting, or electrically and magnetically insulating. Complete results are obtained by making use of the Green's function solution of the multiferroic half-space and the most recently extended method in potential theory (Fabrikant, 1989, 1991; Hanson, 1992a,b). In particular, exact 3D expressions for the coupled MEE fields in the half-space are presented in terms of elementary functions. The physical quantities on the surface of the multiferroic half-space in exact closed forms are also given as special cases.

Discussion is made on the particular condition for vanishing stress singularity at the edge of the spherical or conical indenter. As opposed to the previous one where the mechanically induced part is assumed to be non-singular at the contact edge, this paper assumes that the total stress field has no singularity there. We show that the results for the two different conditions become identical when the electric potential and/or magnetic potential are zero (here 'and/or' depends on the magnetoelectric properties of the indenter). A detailed discussion is given for the piezoelectric materials, which clearly identifies the differences in existing literature.

Apart from the piezoelectric materials, various other decoupled cases are also discussed (see Appendix E). For example, the solution for the piezomagnetic materials can be easily derived from that for the piezoelectric materials since the

magnetic field plays almost the same role as the electric field. Thus, various important discussions related to piezoelectric materials, e.g. on the piezoresponse force microscopy (Kalinin et al., 2004) can be directly borrowed and applied to the piezomagnetic materials.

Some numerical examples are also presented for illustrations. Our results indicate that a complete coupling theory should be used for an accurate prediction of the indentation response, which can be used to characterize the material properties. Our results also show that the coupling among the magnetic, electric and elastic fields provide more feasible ways in controlling the magnitude as well as the distribution of various physical fields in the half-space. This interesting feature could stimulate important applications of advanced technologies such as magnetically writing and electrically reading memory, atomic force microscopy based micro-painting, and ferroelectric/ferromagnetic domain switch.

Acknowledgements

This work was supported by NSFC (Nos. 10725210 and 10832009). It was also partially supported by Air Force Office of Scientific Research under grant AFOSR FA9550-06-1-0317. Financial support from the German Research Foundation (DFG, Project-Nos.: ZH15/14-1 and ZH 15/15-1) is also acknowledged.

Appendix A. The related material coefficients

The four characteristic roots s_i (with real parts) are the solutions of the following eigenequation (Chen et al., 2004):

$$n_0 s^8 - n_1 s^6 + n_2 s^4 - n_3 s^2 + n_4 = 0, \tag{A1}$$

where

$$\begin{aligned}
n_0 &= c_{44}\Pi,\\
n_1 &= c_{11}\Pi + [c_{44}^2 - (c_{13}+c_{44})^2]\Pi_{11} + [c_{44}\varepsilon_{11} + (e_{15}+e_{31})^2]\Pi_{22} + [c_{44}\mu_{11} + (q_{15}+q_{31})^2]\Pi_{33}\\
&\quad + 2[c_{44}e_{15} - (c_{13}+c_{44})(e_{15}+e_{31})]\Pi_{12}\\
&\quad + 2[c_{44}q_{15} - (c_{13}+c_{44})(q_{15}+q_{31})]\Pi_{13} + 2[c_{44}d_{11} + (e_{15}+e_{31})(q_{15}+q_{31})]\Pi_{23},\\
n_2 &= c_{11}(c_{44}\Pi_{11} + e_{15}\Pi_{12} + q_{15}\Pi_{13}) + c_{44}(c_{33}\Gamma_{11} + e_{33}\Gamma_{12} + q_{33}\Gamma_{13}) + [c_{11}c_{33} + c_{44}^2 - (c_{13}+c_{44})^2]\Omega_{11} + (e_{15}+e_{31})^2\Omega_{22}\\
&\quad + (q_{15}+q_{31})^2\Omega_{33} + [c_{11}e_{33} + c_{44}e_{15} - 2(c_{13}+c_{44})(e_{15}+e_{31})]\Omega_{12} + [c_{11}q_{33} + c_{44}q_{15}\\
&\quad - 2(c_{13}+c_{44})(q_{15}+q_{31})]\Omega_{13} + 2(e_{15}+e_{31})(q_{15}+q_{31})\Omega_{23},\\
n_3 &= c_{44}\Gamma + [c_{11}c_{33} - (c_{13}+c_{44})^2]\Gamma_{11} + [c_{11}\varepsilon_{33} + (e_{15}+e_{31})^2]\Gamma_{22} + [c_{11}\mu_{33} + (q_{15}+q_{31})^2]\Gamma_{33}\\
&\quad + 2[c_{11}e_{33} - (c_{13}+c_{44})(e_{15}+e_{31})]\Gamma_{12} + 2[c_{11}q_{33} - (c_{13}+c_{44})(q_{15}+q_{31})]\Gamma_{13} + 2[c_{11}d_{33} + (e_{15}+e_{31})(q_{15}+q_{31})]\Gamma_{23},\\
n_4 &= c_{11}\Gamma,
\end{aligned} \tag{A2}$$

with

$$\begin{aligned}
\Omega_{11} &= \varepsilon_{11}\mu_{33} + \varepsilon_{33}\mu_{11} - 2d_{11}d_{33},\\
\Omega_{22} &= c_{44}\mu_{33} + c_{33}\mu_{11} + 2q_{15}q_{33},\\
\Omega_{33} &= c_{44}\varepsilon_{33} + c_{33}\varepsilon_{11} + 2e_{15}e_{33},\\
\Omega_{12} &= e_{33}\mu_{11} + e_{15}\mu_{33} - d_{11}q_{33} - d_{33}q_{15},\\
\Omega_{13} &= q_{33}\varepsilon_{11} + q_{15}\varepsilon_{33} - d_{11}e_{33} - d_{33}e_{15},\\
\Omega_{23} &= -(c_{44}d_{33} + c_{33}d_{11} + e_{15}q_{33} + e_{33}q_{15}),
\end{aligned}$$

and Π and Γ being the determinants of, Π_{ij} and Γ_{ij} being the cominors of, the corresponding matrices $\boldsymbol{\Pi}$ and $\boldsymbol{\Gamma}$ defined by

$$\boldsymbol{\Pi} = \begin{bmatrix} c_{33} & e_{33} & q_{33}\\ -e_{33} & \varepsilon_{33} & d_{33}\\ -q_{33} & d_{33} & \mu_{33} \end{bmatrix}, \quad \boldsymbol{\Gamma} = \begin{bmatrix} c_{44} & e_{15} & q_{15}\\ -e_{15} & \varepsilon_{11} & d_{11}\\ -q_{15} & d_{11} & \mu_{11} \end{bmatrix}.$$

The eigenequation (A1) includes the decoupled piezoelectric, piezomagnetic, and elastic materials as its special cases. For example, by setting q_{ij}=d_{ij}=0, along μ_{33}=0 and μ_{11}=1 (to remove the eigenvalues associated with the decoupled magnetic field so that the size of the eigenequation is properly reduced) we obtain from Eq. (A2),

$$\begin{aligned}
n_0 &= 0, \quad n_1 = c_{44}(c_{33}\varepsilon_{33} + e_{33}^2),\\
n_2 &= c_{44}(c_{33}\varepsilon_{11} + e_{33}e_{15}) + [c_{11}c_{33} + c_{44}^2 - (c_{13}+c_{44})^2]\varepsilon_{33} + (e_{15}+e_{31})^2 c_{33} + [c_{11}e_{33} + c_{44}e_{15} - 2(c_{13}+c_{44})(e_{15}+e_{31})]e_{33},\\
n_3 &= c_{44}(c_{44}\varepsilon_{11} + e_{15}^2) + [c_{11}c_{33} - (c_{13}+c_{44})^2]\varepsilon_{11} + [c_{11}\varepsilon_{33} + (e_{15}+e_{31})^2]c_{44} + 2[c_{11}e_{33} - (c_{13}+c_{44})(e_{15}+e_{31})]e_{15},\\
n_4 &= c_{11}(c_{44}\varepsilon_{11} + e_{15}^2).
\end{aligned} \tag{A3}$$

Thus, Eq. (A1) becomes

$$n_1 s^6 - n_2 s^4 + n_3 s^2 - n_4 = 0, \tag{A4}$$

which is identical to Eq. (5) in Chen (2000) for piezoelectric materials. Similarly, for piezomagnetic materials, we can set $e_{ij}=d_{ij}=0$, along with $\varepsilon_{33}=0$ and $\varepsilon_{11}=1$ (for removing the decoupled electric field from the eigenequation). We point out that the reduced expressions are actually the same as those for piezoelectric materials if one replaces ε_{ij} and e_{ij} by μ_{ij} and q_{ij}, respectively. The decoupled eigenequation for the purely elastic case can be reduced from Eqs. (A3) and (A4) by further assuming $e_{ij}=0$, along with $\varepsilon_{33}=0$ and $\varepsilon_{11}=1$ (for removing the decoupled electric field from the eigenequation). For this case, we obtain

$$n_2 s^4 - n_3 s^2 + n_4 = 0, \tag{A5}$$

where

$$n_2 = c_{44}c_{33}, \quad n_3 = c_{11}c_{33} - c_{13}^2 - 2c_{13}c_{44}, \quad n_4 = c_{11}c_{44}. \tag{A6}$$

Eq. (A5) is identical to Eq. (2.2.43) in Ding et al. (2006).

The material constants α_{ij} and κ_{ij} can be still expressed the same as those given in Chen et al. (2004):

$$\alpha_{i1} = \kappa_{i2}s_i/\kappa_{i1}, \quad \alpha_{i2} = \kappa_{i3}s_i/\kappa_{i1}, \quad \alpha_{i3} = \kappa_{i4}s_i/\kappa_{i1}, \tag{A7}$$

$$\kappa_{ij} = a_j s_i^6 - b_j s_i^4 + f_j s_i^2 - g_j \quad (j = 1,2,3,4), \tag{A8}$$

where

$$\begin{aligned} a_1 &= -(c_{13}+c_{44})\Pi_{13} + (e_{15}+e_{31})\Pi_{23} + (q_{15}+q_{31})\Pi_{33} \\ b_1 &= -(c_{13}+c_{44})\Omega_{13} + (e_{15}+e_{31})\Omega_{23} + (q_{15}+q_{31})\Omega_{33}, \\ f_1 &= -(c_{13}+c_{44})\Gamma_{13} + (e_{15}+e_{31})\Gamma_{23} + (q_{15}+q_{31})\Gamma_{33}, \\ g_1 &= 0, \end{aligned} \tag{A9}$$

$$\begin{aligned} a_2 &= -c_{44}\Pi_{13}, \\ b_2 &= -c_{11}\Pi_{13} - c_{44}\Omega_{13} - (c_{13}+c_{44})[d_{33}(e_{15}+e_{31}) - \varepsilon_{33}(q_{15}+q_{31})] - (e_{15}+e_{31})[q_{33}(e_{15}+e_{31}) - e_{33}(q_{15}+q_{31})], \\ f_2 &= -c_{11}\Omega_{13} - c_{44}\Gamma_{13} - (c_{13}+c_{44})[d_{11}(e_{15}+e_{31}) - \varepsilon_{11}(q_{15}+q_{31})] - (e_{15}+e_{31})[q_{15}(e_{15}+e_{31}) - e_{15}(q_{15}+q_{31})], \\ g_2 &= -c_{11}\Gamma_{13}, \end{aligned} \tag{A10}$$

$$\begin{aligned} a_3 &= c_{44}\Pi_{23}, \\ b_3 &= c_{11}\Pi_{23} + c_{44}\Omega_{23} + (c_{13}+c_{44})[d_{33}(c_{13}+c_{44}) + e_{33}(q_{15}+q_{31})] + (e_{15}+e_{31})[q_{33}(c_{13}+c_{44}) - c_{33}(q_{15}+q_{31})], \\ f_3 &= c_{11}\Omega_{23} + c_{44}\Gamma_{23} + (c_{13}+c_{44})[d_{11}(c_{13}+c_{44}) + e_{15}(q_{15}+q_{31})] + (e_{15}+e_{31})[q_{15}(c_{13}+c_{44}) - c_{44}(q_{15}+q_{31})], \\ g_3 &= c_{11}\Gamma_{23}, \end{aligned} \tag{A11}$$

$$\begin{aligned} a_4 &= c_{44}\Pi_{33}, \\ b_4 &= c_{11}\Pi_{33} + c_{44}\Omega_{33} - (c_{13}+c_{44})[\varepsilon_{33}(c_{13}+c_{44}) + e_{33}(e_{15}+e_{31})] - (e_{15}+e_{31})[e_{33}(c_{13}+c_{44}) - c_{33}(e_{15}+e_{31})], \\ f_4 &= c_{11}\Omega_{33} + c_{44}\Gamma_{33} - (c_{13}+c_{44})[\varepsilon_{11}(c_{13}+c_{44}) + e_{15}(e_{15}+e_{31})] - (e_{15}+e_{31})[e_{15}(c_{13}+c_{44}) - c_{44}(e_{15}+e_{31})], \\ g_4 &= c_{11}\Gamma_{33}. \end{aligned} \tag{A12}$$

Appendix B. The reciprocity theorem for magneto-electro-elasticity

Here we present within the framework of linear magneto-electro-elasticity a simple derivation of the reciprocity theorem, which will then be used to derive the important relation as shown in Eq. (8). In accordance with the problem studied in the paper, we focus on the static problem only. The derivation for piezoelectric media can be found in Ding and Chen (2001). Li (2003) presented a dynamic reciprocity theorem for a thermo-magneto-electro-elastic medium in which more advanced mathematics are involved.

For a domain V with a surface S in an Euclidean space, we have from the divergence theorem

$$\iiint_V \sigma_{ji}u_{i,j}\,dV = \iint_S n_j\sigma_{ji}u_i\,dS - \iiint_V \sigma_{ji,j}u_i\,dV, \tag{B1}$$

$$\iiint_V D_i\phi_{,i}\,dV = \iint_S n_i D_i\phi\,dS - \iiint_V D_{i,i}\phi\,dV, \tag{B2}$$

$$\iiint_V B_i\psi_{,i}\,dV = \iint_S n_i B_i\psi\,dS - \iiint_V B_{i,i}\psi\,dV. \tag{B3}$$

These are mathematical identities, and the second-order tensor σ_{ij}, the vectors u_i, D_i and B_i, and the scalars ϕ and ψ can be arbitrary (but at least once differentiable in V). In the above equations, the convention of summation over repeated indices (running from 1 to 3) is employed, a comma followed by a subscript, say j, indicates differentiation with respect to the coordinate x_j in a Cartesian coordinate system, and n_i is the directional cosine of an outward normal.

Since σ_{ij} is symmetric, we can obtain by adding Eqs. (B1)–(B3) together the following relation:

$$\iiint_V (\sigma_{ij}s_{ij} - D_iE_i - B_iH_i)\,dV = \iint_S (t_iu_i - \omega_e\phi - \omega_m\psi)\,dS + \iiint_V (f_iu_i - \rho_e\phi - \rho_m\psi)\,dV, \tag{B4}$$

where

$$s_{ij}=(u_{i,j}+u_{j,i})/2,\quad E_i=-\phi_{,i},\quad H_i=-\psi_{,i},$$
$$f_i=-\sigma_{ji,j},\quad \rho_e=D_{i,i},\quad \rho_m=B_{i,i},$$
$$t_i=n_j\sigma_{ji},\quad \omega_e=-n_iD_i,\quad \omega_m=-n_iB_i. \tag{B5}$$

If σ_{ij}, s_{ij}, u_i, D_i, E_i, B_i, H_i, ϕ and ψ are the physical field variables for an MEE body as indicated in the text, f_i, ρ_e, and ρ_m will be the body force vector, the electric charge density and current density, respectively, and t_i, ω_e and ω_m are the surface force vector, surface electric charge and magnetic charge, respectively. We also have the following constitutive relations for a general anisotropic MEE medium:

$$\sigma_{ij}=c_{ijkl}s_{kl}-e_{kij}E_k-q_{kij}H_k,$$
$$D_i=e_{ikl}s_{kl}+\varepsilon_{ik}E_k+d_{ik}H_k,$$
$$B_i=q_{ikl}s_{kl}+d_{ik}E_k+\mu_{ik}H_k, \tag{B6}$$

where the material constants bear the same physical meanings as those in Eq. (1), but without using the compact Voigt notation.

We now consider two states of the MEE body, which correspond to two different groups of external stimuli, respectively. The first will be indicated by superscript (1), while the second by superscript (2). Then, we obtain from Eq. (B4)

$$\iiint_V(\sigma_{ij}^{(1)}s_{ij}^{(2)}-D_i^{(1)}E_i^{(2)}-B_i^{(1)}H_i^{(2)})\,dV=\iint_S(t_i^{(1)}u_i^{(2)}-\omega_e^{(1)}\phi^{(2)}-\omega_m^{(1)}\psi^{(2)})\,dS+\iiint_V(f_i^{(1)}u_i^{(2)}-\rho_e^{(1)}\phi^{(2)}-\rho_m^{(1)}\psi^{(2)})\,dV, \tag{B7}$$

$$\iiint_V(\sigma_{ij}^{(2)}s_{ij}^{(1)}-D_i^{(2)}E_i^{(1)}-B_i^{(2)}H_i^{(1)})\,dV=\iint_S(t_i^{(2)}u_i^{(1)}-\omega_e^{(2)}\phi^{(1)}-\omega_m^{(2)}\psi^{(1)})\,dS+\iiint_V(f_i^{(2)}u_i^{(1)}-\rho_e^{(2)}\phi^{(1)}-\rho_m^{(2)}\psi^{(1)})\,dV. \tag{B8}$$

Noticing Eq. (A6) and the material symmetry properties, one can easily verify that

$$\sigma_{ij}^{(1)}s_{ij}^{(2)}-D_i^{(1)}E_i^{(2)}-B_i^{(1)}H_i^{(2)}=\sigma_{ij}^{(2)}s_{ij}^{(1)}-D_i^{(2)}E_i^{(1)}-B_i^{(2)}H_i^{(1)}. \tag{B9}$$

Thus, we have from Eqs. (B7) and (B8)

$$\iint_S(t_i^{(1)}u_i^{(2)}-\omega_e^{(1)}\phi^{(2)}-\omega_m^{(1)}\psi^{(2)})\,dS+\iiint_V(f_i^{(1)}u_i^{(2)}-\rho_e^{(1)}\phi^{(2)}-\rho_m^{(1)}\psi^{(2)})\,dV$$
$$=\iint_S(t_i^{(2)}u_i^{(1)}-\omega_e^{(2)}\phi^{(1)}-\omega_m^{(2)}\psi^{(1)})\,dS+\iiint_V(f_i^{(2)}u_i^{(1)}-\rho_e^{(2)}\phi^{(1)}-\rho_m^{(2)}\psi^{(1)})\,dV. \tag{B10}$$

This is the mathematical formulation of the reciprocity theorem for an MEE medium. It states that the "work" done by the first group of external stimuli on the second-state "displacements" is equal to the "work" done by the second group of stimuli on the first-state "displacements".

Let us now consider the problem of a transversely isotropic MEE half-space as studied in the text. In the first state, the half-space is subjected to a concentrated vertical force P only at the origin, so that we have $t_3^{(1)}=P\delta(x_1)\delta(x_2)$, where the x_1- and x_2-axes of the Cartesian coordinates are located on the surface while the x_3-axis pointing into the half-space. In the second state, the half-space is subjected to a positive point free charge Q only at the origin, so that we have $\omega_e^{(2)}=Q\delta(x_1)\delta(x_2)$. Then, Eq. (B10) gives

$$Pu_z^{(2)}(0,0,0)=-Q\phi^{(1)}(0,0,0). \tag{B11}$$

On the other hand, from Eq. (4) we have

$$\phi^{(1)}(0,0,0)=\xi_{21}P,\quad u_z^{(2)}(0,0,0)=-\xi_{12}Q. \tag{B12}$$

Thus we obtain $\xi_{21}=\xi_{12}$. Other relations can be obtained similarly, and hence we have Eq. (8) in the text.

Appendix C. The solution to integral equation (16)

We first rewrite Eq. (16) as

$$\int_0^{2\pi}\int_0^a\frac{p_j(\rho,\theta_0)}{R_0}\rho\,d\rho\,d\theta_0=\frac{1}{\eta}\sum_{k=1}^{3}\eta_{kj}w_k(r,\theta,0)\quad(j=1,2,3).$$

According to Fabrikant (1989), this equation can be transformed into

$$4\int_0^r\frac{dx}{(r^2-x^2)^{1/2}}\int_x^a\frac{\rho d\rho}{(\rho^2-x^2)^{1/2}}L\left(\frac{x^2}{r\rho}\right)p_j(\rho,\theta)=q_j(r,\theta)\quad(j=1,2,3), \tag{C1}$$

where $q_j=(1/\eta)\sum_{k=1}^{3}\eta_{kj}w_k(r,\theta,0)$, and

$$L(k)f(\theta)=\frac{1}{2\pi}\int_0^{2\pi}\lambda(k,\theta-\theta_0)f(\theta_0)\,d\theta_0 \tag{C2}$$

is the Poisson operator, with

$$\lambda(k,\theta)=\frac{1-k^2}{1+k^2-2k\cos\theta}. \tag{C3}$$

Then the solution to Eq. (C1) can be obtained by inverting two Abel operators and one Poisson operator as (Fabrikant, 1989)

$$p_j(r,\theta,0)=\frac{1}{\pi^2}\left[\frac{\chi_j(a,r,\theta)}{\sqrt{a^2-r^2}}-\int_r^a\frac{dt}{\sqrt{t^2-r^2}}\frac{d}{dt}\chi_j(t,r,\theta)\right], \tag{C4}$$

where

$$\chi_j(t,r,\theta)=\frac{1}{t}\int_0^t\frac{xdx}{\sqrt{t^2-x^2}}\frac{d}{dx}\left[xL\left(\frac{xr}{t^2}\right)q_j(x,\theta)\right]. \tag{C5}$$

It can be seen that the first term on the right-hand side of Eq. (C4) will be singular at $r=a$ if $\chi_j(a, a, \theta)$ does not vanish there. For the three indenters considered in the text, we can obtain

$$\chi_j(t,r,\theta)=\begin{cases} q_{0j}, & \text{for } flat \\ q_{0j}-\dfrac{\pi t}{2}\dfrac{\eta_{1j}}{\eta}\cot\beta, & \text{for cone,} \\ q_{0j}-\dfrac{\eta_{1j}}{\eta}\dfrac{t^2}{R}, & \text{for sphere,} \end{cases} \tag{C6}$$

where

$$q_{0j}=\frac{1}{\eta}(\eta_{1j}h+\eta_{2j}\phi_0+\eta_{3j}\psi_0).$$

For a conical or spherical indenter, a usual requirement is that there is no stress singularity at $r=a$. This leads to the following relation:

$$q_{01}-\frac{\pi a}{2}\frac{\eta_{11}}{\eta}\cot\beta=0 \tag{C7}$$

for the conical indenter, and

$$q_{01}-\frac{\eta_{11}}{\eta}\frac{a^2}{R}=0 \tag{C8}$$

for the spherical indenter. These relations determine the contact radii for the two indenters. It should be noted that, in our previous works for piezoelectric materials (Chen and Ding, 1999; Chen et al., 1999), it was assumed that the stress singularity disappears when the electric potential is zero (i.e. $\phi_0=0$). Under such a condition (for the MEE material, also $\psi_0=0$), we can obtain from Eq. (C7) $h=\pi a\cot\beta/2$ for the conical indenter and from Eq. (C8) $h=a^2/R$ for the spherical indenter. These relations are identical to those for pure elasticity (Hanson, 1992a,b). Using the correspondence principle (Karapetian et al., 2002), Kalinin et al. (2004) and Karapetian et al. (2005) also obtained these classical results as in Chen and Ding (1999) and Chen et al. (1999). In this paper, however, we use Eqs. (C7) or (C8) to determine the contact radius for the electrically and magnetically conducting conical or spherical indenter, see Eqs. (26) and (31) in the text. This means that there is entirely no stress singularity at $r=a$ under a combination of mechanical, electrical, and magnetic actions. Although it sounds theoretically more reasonable, experiment-based verification is still desired.

Substituting $\chi_j(t, r, \theta)$ in Eq. (C6) into Eq. (C4) leads to Eqs. (18), (23), and (28) for the flat, conical and spherical indenters, respectively. To obtain the exact expressions for the 3D coupled field in the half-space as presented in Appendix D, the results of Fabrikant (1989) and Hanson (1992a,b) should be further employed.

Solutions to Eqs. (34) and (54) can be obtained similarly, and they are omitted here for brevity.

Appendix D. Exact 3D MEE field in the half-space due to different indenters

D.1. Flat-ended indenter

The complete 3D solutions of the MEE half-space under a flat-ended indenter are

$$u_r=-\frac{2\pi a}{r}\sum_{i=1}^{4}A_i\left[1-\frac{(a^2-l_{1i}^2)^{1/2}}{a}\right],$$

$$w_k=2\pi\sum_{i=1}^{4}\alpha_{ik}A_i\sin^{-1}\left(\frac{a}{l_{2i}}\right),$$

$$\sigma_{zm} = -2\pi \sum_{i=1}^{4} \gamma_{im} A_i \frac{(a^2 - l_{1i}^2)^{1/2}}{l_{2i}^2 - l_{1i}^2},$$
$$\tau_{zk} = -2\pi \sum_{i=1}^{4} \gamma_{ik} s_i A_i \frac{l_{1i}(l_{2i}^2 - a^2)^{1/2}}{l_{2i}(l_{2i}^2 - l_{1i}^2)},$$
$$\sigma_2 = -4\pi c_{66} \sum_{i=1}^{4} A_i \left\{ \frac{(a^2 - l_{1i}^2)^{1/2}}{l_{2i}^2 - l_{1i}^2} - \frac{2a}{r^2} \left[1 - \frac{(a^2 - l_{1i}^2)^{1/2}}{a} \right] \right\}, \tag{D1}$$

where k=1, 2, 3, m=1, 2, 3, 4, and

$$l_{1i} = \frac{1}{2} \left\{ [(r+a)^2 + z_i^2]^{1/2} - [(r-a)^2 + z_i^2]^{1/2} \right\},$$
$$l_{2i} = \frac{1}{2} \left\{ [(r+a)^2 + z_i^2]^{1/2} + [(r-a)^2 + z_i^2]^{1/2} \right\}. \tag{D2}$$

Since at z=0,

$$l_{1i} \to \min(a,r), \quad l_{2i} \to \max(a,r), \tag{D3}$$

and we have from Eq. (7) the relation $\sum_{i=1}^{4} \gamma_{ik} I_{ij} = \delta_{kj}/(2\pi)$, further by noticing Eq. (18), Eq. (15) can be recovered exactly. Such and other inspections can be easily performed to verify the correctness of the above expressions. The coefficients A_i in Eq. (D1) are determined by the given electric and magnetic conditions, as given below.

D.1.1. For the flat indenter under the electrically and magnetically conducting condition, we have

$$A_i = \sum_{j=1}^{3} \frac{C_{ij}(\eta_{1j} h + \eta_{2j} \phi_0 + \eta_{3j} \psi_0)}{\pi^2 \eta} \quad (i = 1,2,3,4). \tag{D4}$$

D.1.2. For the flat indenter under the electrically conducting and magnetically insulating condition, there will be no magnetic source contribution to the MEE field in the half-space, and for this case, we obtain

$$A_i = I_{i1} \frac{\xi_{22} h - \xi_{12} \phi_0}{\pi^2 \eta_{33}} + I_{i2} \frac{-\xi_{21} h + \xi_{11} \phi_0}{\pi^2 \eta_{33}} \quad (i = 1,2,3,4). \tag{D5}$$

D.1.3. For the flat indenter under the electrically insulating and magnetically conducting condition, there will be no electric source contribution to the MEE field in the half-space, and for this case, we have

$$A_i = I_{i1} \frac{\xi_{33} h - \xi_{13} \psi_0}{\pi^2 \eta_{22}} + I_{i2} \frac{-\xi_{31} h + \xi_{11} \psi_0}{\pi^2 \eta_{22}} \quad (i = 1,2,3,4). \tag{D6}$$

D.1.4. For the flat indenter under the electrically and magnetically insulating condition, only the pressure under the indenter contributes to the MEE field in the half-space, and for this case, we have

$$A_i = \frac{I_{i1} h}{\pi^2 \xi_{11}} \quad (i = 1,2,3,4). \tag{D7}$$

D.2. Conical indenter

In accordance with Eq. (23), we divide the complete 3D solution into two parts: the first part is due to the first term (i.e. mechanical part) and indicated by superscript I, and the second part corresponds to the second term (i.e. indentation by the electromagnetic means) and indicated by superscript II. The results are

$$u_r^I = -\cot\beta \sum_{i=1}^{4} A_i^I \left\{ \frac{(r l_{2i} - 2a l_{1i})(l_{2i}^2 - r^2)^{1/2}}{2r^2} + \frac{r}{2} \ln\left[l_{2i} + (l_{2i}^2 - r^2)^{1/2} \right] - \frac{z_i (r^2 + z_i^2)^{1/2}}{2r} - \frac{r}{2} \ln\left[z_i + (z_i^2 + r^2)^{1/2} \right] + \frac{a^2}{2r} \right\},$$
$$w_k^I = \cot\beta \sum_{i=1}^{4} \alpha_{ik} A_i^I \left\{ a \sin^{-1}\left(\frac{a}{l_{2i}} \right) + (l_{2i}^2 - a^2)^{1/2} - (r^2 + z_i^2)^{1/2} - z_i \ln\left[l_{2i} + (l_{2i}^2 - r^2)^{1/2} \right] + z_i \ln\left[z_i + (r^2 + z_i^2)^{1/2} \right] \right\},$$
$$\sigma_{zm}^{\mathrm{I}} = -\cot\beta \sum_{i=1}^{4} \gamma_{im} A_i^I \left\{ \ln[l_{2i} + (l_{2i}^2 - r^2)^{1/2}] - \ln\left[z_i + (z_i^2 + r^2)^{1/2} \right] \right\},$$
$$\tau_{zk}^{\mathrm{I}} = \cot\beta \sum_{i=1}^{4} \gamma_{ik} s_i A_i^I \frac{(l_{2i}^2 - a^2)^{1/2} - (r^2 + z_i^2)^{1/2}}{r},$$
$$\sigma_2^{\mathrm{I}} = -2c_{66} \cot\beta \sum_{i=1}^{4} A_i^I \left[\frac{(2a^2 - l_{2i}^2)(a^2 - l_{1i}^2)^{1/2}}{a r^2} + \frac{z_i (r^2 + z_i^2)^{1/2} - a^2}{r^2} \right], \tag{D8}$$

$$u_r^{\mathrm{II}} = -\frac{2\pi a}{r} \sum_{i=1}^{4} A_i^{II} \left[1 - \frac{(a^2 - l_{1i}^2)^{1/2}}{a} \right],$$

$$w_k^{\mathrm{II}} = 2\pi \sum_{i=1}^{4} \alpha_{ik} A_i^{II} \sin^{-1}\left(\frac{a}{l_{2i}}\right),$$
$$\sigma_{zm}^{\mathrm{II}} = -2\pi \sum_{i=1}^{4} \gamma_{im} A_i^{II} \frac{(a^2-l_{1i}^2)^{1/2}}{l_{2i}^2-l_{1i}^2},$$
$$\tau_{zk}^{\mathrm{II}} = -2\pi \sum_{i=1}^{4} \gamma_{ik} s_i A_i^{II} \frac{l_{1i}(l_{2i}^2-a^2)^{1/2}}{l_{2i}(l_{2i}^2-l_{1i}^2)},$$
$$\sigma_2^{\mathrm{II}} = -4\pi c_{66} \sum_{i=1}^{4} A_i^{II} \left\{ \frac{(a^2-l_{1i}^2)^{1/2}}{l_{2i}^2-l_{1i}^2} - \frac{2a}{r^2}\left[1-\frac{(a^2-l_{1i}^2)^{1/2}}{a}\right]\right\}. \tag{D9}$$

The coefficients A_i in Eqs. (D8) and (D9) are determined by the given electric and magnetic conditions, as given below.

D.2.1. For the conical indenter under the electrically and magnetically conducting condition, we have

$$A_i^{I} = \sum_{j=1}^{3} I_{ij} \frac{\eta_{1j}}{\eta}, \quad A_i^{\mathrm{II}} = \sum_{j=1}^{3} I_{ij} \frac{\eta_{1j}(h-a\pi\cot\beta/2)+\eta_{2j}\phi_0+\eta_{3j}\psi_0}{\pi^2\eta}, \quad (i=1,2,3,4). \tag{D10}$$

D.2.2. For the conical indenter under the electrically conducting and magnetically insulating condition, there will be no magnetic source contribution to the MEE field in the half-space, and for this case, we have

$$A_i^{I} = I_{i1}\frac{\xi_{22}}{\eta_{33}} - I_{i2}\frac{\xi_{21}}{\eta_{33}}, \quad A_i^{\mathrm{II}} = I_{i2}\frac{\phi_0}{\pi^2\xi_{22}} \quad (i=1,2,3,4). \tag{D11}$$

where the relation $\eta_{33} = \xi_{11}\xi_{22} - \xi_{12}^2$ has been used.

D.2.3. For the conical indenter under the electrically insulating and magnetically conducting condition, there will be no electric source contribution to the MEE field in the half-space, and for this case, we have

$$A_i^{I} = I_{i1}\frac{\xi_{33}}{\eta_{22}} - I_{i3}\frac{\xi_{31}}{\eta_{22}}, \quad A_i^{\mathrm{II}} = I_{i3}\frac{\psi_0}{\pi^2\xi_{33}} \quad (i=1,2,3,4). \tag{D12}$$

D.2.4 For the conical indenter under the electrically and magnetically insulating condition, only the pressure under the indenter contributes to the MEE field in the half-space, and for this case, we have

$$A_i^{I} = \frac{I_{i1}}{\xi_{11}}, \quad A_i^{II} = 0 \quad (i=1,2,3,4). \tag{D13}$$

D.3. Spherical indenter

In accordance with Eq. (28), and similar to the conical indenter case, we also divide the complete 3D solution into two parts (I and II) as given below:

$$u_r^{I} = -\frac{2r}{\pi R}\sum_{i=1}^{4} A_i^{I}\left[-z_i \sin^{-1}\left(\frac{a}{l_{2i}}\right) + (a^2-l_{1i}^2)^{1/2}\left(1-\frac{l_{1i}^2+2a^2}{3r^2}\right) + \frac{2a^3}{3r^2}\right],$$
$$w_k^{I} = \frac{1}{\pi R}\sum_{i=1}^{4} \alpha_{ik} A_i^{I}\left[(2a^2+2z_i^2-r^2)\sin^{-1}\left(\frac{a}{l_{2i}}\right) + \frac{3l_{1i}^2-2a^2}{a}(l_{2i}^2-a^2)^{1/2}\right],$$
$$\sigma_{zm}^{\mathrm{I}} = \frac{4}{\pi R}\sum_{i=1}^{4} \gamma_{im} A_i^{I}\left[z_i \sin^{-1}\left(\frac{a}{l_{2i}}\right) - (a^2-l_{1i}^2)^{1/2}\right],$$
$$\tau_{zk}^{\mathrm{I}} = \frac{2r}{\pi R}\sum_{i=1}^{4} \gamma_{ik} s_i A_i^{I}\left[-\sin^{-1}\left(\frac{a}{l_{2i}}\right) + \frac{a(l_{2i}^2-a^2)^{1/2}}{l_{2i}^2}\right],$$
$$\sigma_2^{\mathrm{I}} = -\frac{8c_{66}}{3\pi A R r^2}\sum_{i=1}^{4} A_i^{I}[-2a^3 + (l_{1i}^2+2a^2)(a^2-l_{1i}^2)^{1/2}], \tag{D14}$$

$$u_r^{\mathrm{II}} = -\frac{2\pi a}{r}\sum_{i=1}^{4} A_i^{II}\left[1-\frac{(a^2-l_{1i}^2)^{1/2}}{a}\right],$$
$$w_k^{\mathrm{II}} = 2\pi \sum_{i=1}^{4} \alpha_{ik} A_i^{II} \sin^{-1}\left(\frac{a}{l_{2i}}\right),$$
$$\sigma_{zm}^{\mathrm{II}} = -2\pi \sum_{i=1}^{4} \gamma_{im} A_i^{II} \frac{(a^2-l_{1i}^2)^{1/2}}{l_{2i}^2-l_{1i}^2},$$
$$\tau_{zk}^{\mathrm{II}} = -2\pi \sum_{i=1}^{4} \gamma_{ik} s_i A_i^{II} \frac{l_{1i}(l_{2i}^2-a^2)^{1/2}}{l_{2i}(l_{2i}^2-l_{1i}^2)},$$

$$\sigma_2^{\mathrm{II}} = -4\pi c_{66} \sum_{i=1}^{4} A_i^{II} \left\{ \frac{(a^2-l_{1i}^2)^{1/2}}{l_{2i}^2-l_{1i}^2} - \frac{2a}{r^2}\left[1-\frac{(a^2-l_{1i}^2)^{1/2}}{a}\right]\right\}. \tag{D15}$$

D.3.1. For the spherical indenter under the electrically and magnetically conducting condition, we have

$$A_i^I = \sum_{j=1}^{3} I_{ij}\frac{\eta_{1j}}{\eta}, \quad A_i^{\mathrm{II}} = \sum_{j=1}^{3} I_{ij}\frac{\eta_{1j}(h-a^2/R)+\eta_{2j}\phi_0+\eta_{3j}\psi_0}{\pi^2\eta} \quad (i=1,2,3,4). \tag{D16}$$

D.3.2. For the spherical indenter under the electrically conducting and magnetically insulating condition, there will be no magnetic source contribution to the MEE field in the half-space, and for this case, we have

$$A_i^I = I_{i1}\frac{\xi_{22}}{\eta_{33}} - I_{i2}\frac{\xi_{21}}{\eta_{33}}, \quad A_i^{\mathrm{II}} = I_{i2}\frac{\phi_0}{\pi^2\xi_{22}} \quad (i=1,2,3,4), \tag{D17}$$

where the relation $\eta_{33} = \xi_{11}\xi_{22} - \xi_{12}^2$ has also been used.

D.3.3. For the spherical indenter under the electrically insulating and magnetically conducting condition, there will be no electric source contribution to the MEE field in the half-space, and for this case, we have

$$A_i^I = I_{i1}\frac{\xi_{33}}{\eta_{22}} - I_{i3}\frac{\xi_{31}}{\eta_{22}}, \quad A_i^{\mathrm{II}} = I_{i3}\frac{\psi_0}{\pi^2\xi_{33}} \quad (i=1,2,3,4). \tag{D18}$$

D.3.4. For the spherical indenter under the electrically and magnetically insulating condition, only the pressure under the indenter contributes to the MEE field in the half-space, and for this case, we have

$$A_i^I = \frac{I_{i1}}{\xi_{11}}, \quad A_i^{II} = 0 \quad (i=1,2,3,4). \tag{D19}$$

Appendix E. Various decoupled and degenerated cases

E.1. $q_{ij}=d_{ij}=0$

In this case, a magnetic field (for a magnetic half-space) will completely decouple from the coupled electroelastic field (for the piezoelectric half-space). With regard to the electroelastic field, the form of the Green's functions in Eq. (4) keeps unaltered except that the summation is from 1 to 3. The associated three characteristic roots (s_1, s_2 and s_3) are governed by Eq. (A4) in Appendix A. The other equations could be derived using appropriate degeneration procedures from those given in the text. It is noted that the results for a spherical or conical indenter will be different from those obtained in the previous works (Chen and Ding, 1999; Chen et al., 1999) and those obtained by the correspondence principle (Kalinin et al., 2004; Karapetian et al., 2005), but the main difference seems to be only in the relation between the indentation depth and the contact radius of the spherical or conical indenter.

On the other hand, the separated magnetic field in the magnetic half-space is governed by

$$\left(\Delta + \frac{\partial^2}{\partial z_4^2}\right)\psi = 0, \tag{E1}$$

where $s_4 = \sqrt{\mu_{11}/\mu_{33}}$. For a magnetic charge M applied at the origin on the surface, we have

$$\psi = A_4\frac{1}{R_4}, \quad B_z = \mu_{33}s_4A_4\frac{z_4}{R_4^3}, \quad B_r = \mu_{33}s_4^2A_4\frac{r}{R_4^3}, \tag{E2}$$

where $A_4=M/(2\pi\mu_{33}s_4)$. Since no mechanical deformation is involved in this sub-problem, the radius of the contact area should be identical to that in the sub-problem of the piezoelectric half-space, and hence a can be regarded as known *a priori*.

For a magnetically conducting indenter, the governing equation is

$$\psi(r,\theta,0) = \xi_{33}\int_0^{2\pi}\int_0^a \frac{p_3(\rho,\theta_0)}{R_0}\rho\, d\rho\, d\theta_0, \tag{E3}$$

where $\xi_{33}=-1/(2\pi\mu_{33}s_4)$ with the minus sign corresponding to $p_3=-B_z$ as in the text. The solution then can be obtained, similar to that for a flat indenter, as

$$p_3(r,\theta) = \frac{\psi_0}{\pi^2\xi_{33}}\frac{1}{\sqrt{a^2-r^2}}, \tag{E4}$$

which shows that a singularity exists in the magnetic field at the contact edge. Thus, we have in the half-space

$$\psi = \frac{2\psi_0}{\pi}\sin^{-1}\left(\frac{a}{l_{24}}\right), \quad B_z = \frac{2\mu_{33}s_4\psi_0}{\pi}\frac{(a^2-l_{14}^2)^{1/2}}{l_{24}^2-l_{14}^2}, \quad B_r = \frac{2\mu_{11}\psi_0}{\pi}\frac{l_{14}(l_{24}^2-a^2)^{1/2}}{l_{24}(l_{24}^2-l_{14}^2)}. \tag{E5}$$

Note that all these equations also could be derived using an appropriate degeneration procedures from those presented in the text as well as in Appendix D. For example, if we keep in Eq. (D1) only those corresponding to s_4, and remember that $\alpha_{43}=1$, $\gamma_{43}=-\mu_{33}s_4$, $\eta_{13}=\eta_{23}=0$, and $\eta_{33}/\eta=\xi_{33}=-1/(2\pi\mu_{33}s_4)$, then we have $I_{43}=1/(2\pi\gamma_{43})$ and $A_4=\psi_0/\pi^2$, and in turn obtain Eq. (E5) from Eq. (D1).

For a magnetically insulating indenter, the magnetic field in the half-space is null.

E.2. $e_{ij}=d_{ij}=0$

Similarly, an electric field in the half-space is completely separated from the coupled magneto-elastic field. The root of $s_4=\sqrt{\varepsilon_{11}/\varepsilon_{33}}$ then characterizes the separated electric field of the rigid dielectric half-space. Solutions for this case can be easily obtained from Eqs. (E1)–(E4) by changing the involved parameters and field variables from magnetic to electric ones. Other discussions are also similar to those for $q_{ij}=d_{ij}=0$. Note that Giannakopoulos and Parmaklis (2007) presented the solution for a flat-ended and cylindrical punch on a transversely isotropic piezomagnetic half-space by using the Hankel transform method; but explicit expressions were only derived for some physical variables at the surface of the half-space.

E.3. $q_{ij}=e_{ij}=d_{ij}=0$

In this case, both the electric and magnetic fields in the half-space are separated from the elastic field, and they are also separated from each other. The two roots $s_3=\sqrt{\mu_{11}/\mu_{33}}$ and $s_4=\sqrt{\varepsilon_{11}/\varepsilon_{33}}$ will characterize the independent magnetic and electric fields of the magnetic and dielectric half-space, respectively. The results for the separated electric and magnetic fields are the same as those discussed above. The elastic results will be identical to those of Fabrikant (1989) for the flat indenter, and those of Hanson (1992a,b) for the conical and spherical indenters.

References

Benveniste, Y., 1995. Magnetoelectric effect in fibrous composites with piezoelectric and piezomagnetic phases. Phys. Rev. B. 51, 16424–16427.

Chen, W.Q., 2000. On piezoelectric contact problem for a smooth punch. Int. J. Solids Struct. 37, 2331–2340.

Chen, W.Q., Ding, H.J., 1999. Indentation of a transversely isotropic piezoelectric half-space by a rigid sphere. Acta Mech. Solida Sin. 12, 114–120.

Chen, W.Q., Lee, K.Y., 2003. Alternative state space formulations for magnetoelectric thermoelasticity with transverse isotropy and the application to bending analysis of nonhomogeneous plates. Int. J. Solids Struct. 40, 5689–5705.

Chen, W.Q., Lee, K.Y., Ding, H.J., 2004. General solution for transversely isotropic magneto-electro-thermo-elasticity and the potential theory method. Int. J. Eng. Sci. 42, 1361–1379.

Chen, W.Q., Shioya, T., Ding, H.J., 1999. The elasto-electric field for a rigid conical punch on a transversely isotropic piezoelectric half-space. J. Appl. Mech. 66, 764–771.

Ding, H.J., Chen, W.Q., 2001. Three Dimensional Problems of Piezoelasticity. Nova Science Publishers, New York.

Ding, H.J., Chen, W.Q., Zhang, L.C., 2006. Elasticity of Transversely Isotropic Materials. Springer, Dordrecht, The Netherlands.

Fabrikant, V.I., 1989. Applications of Potential Theory in Mechanics: a Selection of New Results. Kluwer Academic Publishers, The Netherlands.

Fabrikant, V.I., 1991. Mixed Boundary Value Problems of Potential Theory and their Applications in Engineering. Kluwer Academic Publishers, The Netherlands.

Feng, W.J., Pan, E., Wang, X., 2007. Dynamic fracture analysis of a penny-shaped crack in a magnetoelectroelastic layer. Int. J. Solids Struct. 44, 7955–7974.

Gao, H., Chiu, C.H., Lee, J., 1992. Elastic contact versus indentation modeling of multi-layered materials. Int. J. Solids Struct. 29, 2471–2492.

Giannakopoulos, A.E., 2000. Strength analysis of spherical indentation of piezoelectric materials. J. Appl. Mech. 67, 409–416.

Giannakopoulos, A.E., Parmaklis, A.Z., 2007. The contact problem of a circular rigid punch on piezomagnetic materials. Int. J. Solids Struct. 44, 4593–4612.

Giannakopoulos, A.E., Suresh, S., 1999. Theory of indentation of piezoelectric materials. Acta Mater. 47, 2153–2164.

Gladwell, G.M.L., 1980. Contact Problems in the Classical Theory of Elasticity. Sijthoff and Noordhoff, The Netherland.

Hanson, M.T., 1992a. The elastic field for conical indentation including sliding friction for transverse isotropy. J. Appl. Mech. 59, S123–S130.

Hanson, M.T., 1992b. The elastic field for spherical Hertzian contact including sliding friction for transverse isotropy. J. Tribol. 114, 604–610.

Hanson, M.T., Puja, I.W., 1997. The elastic field resulting from elliptical Hertzian contact of transversely isotropic bodies: closed-form solutions for normal and shear loading. J. Appl. Mech. 64, 457–465.

Hou, P.F., Leung, A.Y.T., Ding, H.J., 2003. The elliptical Hertzian contact of transversely isotropic magnetoelectroelastic bodies. Int. J. Solids Struct. 40, 2833–2850.

Hou, P.F., Ding, H.J., Chen, J.Y., 2005. Green's functions for transversely isotropic magnetoelectroelastic media. Int. J. Eng. Sci. 43, 826–858.

Johnson, K.L., 1985. Contact Mechanics. Cambridge University Press, Cambridge.

Kalinin, S.V., Bonnell, D.A., 2002. Imaging mechanism of piezoresponse force microscopy of ferroelectric surfaces. Phys. Rev. B 65, 125408.

Kalinin, S.V., Karapetian, E., Kachanov, M., 2004. Nanoelectromechanics of piezoresponse force microscopy. Phys. Rev. B 70, 184101.

Kalinin, S.V., Mirman, B., Karapetian, E., 2007a. Relationship between direct and converse piezoelectric effect in a nanoscaled electromechanical contact. Phys. Rev. B 76, 212102.

Kalinin, S.V., Rodriguez, B.J., Jesse, S., Karapetian, E., Mirman, B., Eliseev, E.A., Morozovska, A.N., 2007b. Nanoscale electromechanics of ferroelectric and biological systems: a new dimension in scanning probe microscopy. Annu. Rev. Mater. Res. 37, 189–238.

Karapetian, E., Kachanov, M., Kalinin, S.V., 2005. Nanoelectromechanics of piezoelectric indentation and applications to scanning probe microscopies of ferroelectric materials. Phil. Mag. 85, 1017–1051.

Karapetian, E., Kachanov, M., Kalinin, S.V., 2009. Stiffness relations for piezoelectric indentation of flat and non-flat punches of arbitrary planform: applications to probing nanoelectromechanical properties of materials. J. Mech. Phys. Solids 57, 673–688.

Karapetian, E., Kachanov, M., Sevostianov, I., 2002. The principle of correspondence between elastic and piezoelectric problems. Arch. Appl. Mech. 72, 564–587.

Lawn, B.R., Wilshaw, T.R., 1975. Review, indentation fracture: principles and applications. J. Mater. Sci. 10, 1049–1081.

Li, J.Y., 2003. Uniqueness and reciprocity theorems for linear thermo-electro-magneto-elasticity. Q. J. Mech. Appl. Math. 56, 35–43.

Li, J.Y., Dunn, M.L., 1998. Micromechanics of magnetoelectroelastic composite materials: average fields and effective behavior. J. Intell. Mater. Syst. Struct. 7, 404–415.

Liu, J.X., Liu, X.L., Zhao, Y.B., 2001. Green's functions for anisotropic magneto-electro-elastic solids with an elliptical cavity or a crack. Int. J. Eng. Sci. 39, 1405–1418.

Nan, C.W., 1994. Magnetoelectric effect in composites of piezoelectric and piezomagnetic phases. Phys. Rev. B B50, 6082–6088.
Nan, C.W., Bichurin, M.I., Dong, S.X., Viehland, D., Srinivasan, G., 2008. Multiferroic magnetoelectric composites: historical perspective, status, and future directions. J. Appl. Phys. 103, 031101.
Pan, E., 2001. Exact solution for simply supported and multilayered magneto-electro-elastic plates. J. Appl. Mech. 68, 608–618.
Pan, E., 2002. Three-dimensional Green's functions in anisotropic magneto-electro-elastic bimaterials. Z. Angew. Math. Phys. 53, 815–838.
Pan, E., Wang, R., 2009. Effects of geometric size and mechanical boundary conditions on magnetoelectric coupling in multiferroic composites. J. Phys. D: Appl. Phys. 42, 245503.
Petrov, V.M., Srinivasan, G., 2008. Enhancement of magnetoelectric coupling in functionally graded ferroelectric and ferromagnetic bilayers. Phys. Rev. B78, 184421.
Sackfield, A., Hills, D.A., Nowell, D., 1993. Mechanics of Elastic Contacts. Butterworth-Heinemann, London.
Sih, G.C., Chen, E.P., 2003. Dilatational and distortional behavior of cracks in magnetoelectroelastic materials. Theor. Appl. Fract. Mech. 40, 1–21.
Sneddon, I.N., 1965. The relation between load and penetration in the axisymmetric Boussinesq problem for a punch of arbitrary profile. Int. J. Eng. Sci. 3, 47–57.
Spaldin, N.A., Fiebig, M., 2005. The renaissance of magnetoelectric multiferroics. Science 309, 391–392.
Vlassak, J.J., Ciavarella, M., Barber, J.R., Wang, X., 2003. The indentation modulus of elastically anisotropic materials for indenters of arbitrary shape. J. Mech. Phys. Solids 51, 1701–1721.
Wang, J.H., Chen, C.Q., Lu, T.J., 2008. Indentation responses of piezoelectric films. J. Mech. Phys. Solids 56, 3331–3351.
Wang, X., Shen, Y.P., 2002. The general solution of three-dimensional problems in magnetoelectroelastic media. Int. J. Eng. Sci. 40, 1069–1080.
Wang, X., Pan, E., Albrecht, J.D., 2008. Two-dimensional Green's functions in anisotropic multiferroic bimaterials with a viscous interface. J. Mech. Phys. Solids 56, 2863–2875.
Wu, T.L., Huang, J.H., 2000. Closed-form solutions for the magnetoelectric coupling coefficients in fibrous composites with piezoelectric and piezomagnetic phase. Int. J. Solids Struct. 37, 2981–3009.
Yang, F.Q., 2008. Analysis of the axisymmetric indentation of a semi-infinite piezoelectric material: the evaluation of the contact stiffness and the effective piezoelectric constant. J. Appl. Phys. 103, 074115.
Yu, H.Y., 2001. A concise treatment of indentation problems in transversely isotropic half-spaces. Int. J. Solids Struct. 38, 2213–2232.